UNIVERSITY OF OKLAHOMA

GRADUATE COLLEGE

IMPLEMENTING FIBER-REINFORCED, SELF-CONSOLIDATING CONCRETE AS A REPAIR MATERIAL FOR AASHTO PRESTRESSED CONCRETE GIRDERS

A THESIS

SUBMITTED TO THE GRADUATE FACULTY

in partial fulfillment of the requirements for the

Degree of

MASTER OF SCIENCE

By

JACOB G. CHOATE
Norman, Oklahoma
2018

IMPLEMENTING FIBER-REINFORCED, SELF-CONSOLIDATING CONCRETE AS A REPAIR MATERIAL FOR AASHTO PRESTRESSED CONCRETE GIRDERS

A THESIS APPROVED FOR THE
SCHOOL OF CIVIL ENGINEERING AND ENVIRONMENTAL SCIENCE

BY

_____
Dr. Jeffery S. Volz, Chair

_____
Dr. Royce W. Floyd

_____
Dr. P. Scott Harvey Jr.

Dedication

In 1966, a few months before the passing of a true American idol, a video was assembled that documented the idea and plans for a futuristic utopia capable of showcasing to the rest of the world the potential and practicality of innovation. The city was arranged and imagined by the some of the most pioneering experts of design and engineering of the time. As such, this "Experimental Prototype Community of Tomorrow" included the planned implementation of some of the most technically advanced feats of architecture, planning, and engineering even by today's standards. If this city's dreamer had been alive to see it through to fruition, it would be an inspiration to the rest of the world and a true testament to the wondrous possibilities that we, as a people, can accomplish together.

The concept behind this "World of Tomorrow" embraces creative and technical ideologies of current industries while also promoting the essentiality of both inspiration and the acquisition of knowledge for the betterment of society. The research presented in this document is dedicated to that idea. The idea that we are to not just pass on the knowledge and understanding we possess, but to continuously push the limits of possibility to new altitudes. And, by doing so, we open the door to opportunities limited only by the scope of our imagination. The future is rooted in imagination and curiosity, which breed new ideas, paving new paths toward a brighter tomorrow. As long as there are paths to explore, we can keep moving forward.

Acknowledgements

As much as I would like to take credit for this work and for all that it took to produce it, I simply cannot. All the good that came to me was graciously given by family, friends, and professional colleagues. Collectively, they are responsible for any admirable qualities that I possess.

First, I want to acknowledge my family for being the support that I need, despite any faults or shortcomings I have had. It is beyond a shadow of a doubt, I would not have been able to reach this milestone without the motivation they gave me to keep moving forward. In addition, special acknowledgements are in order for both my parents, Jack and Julie, and my closest companion, Dianna, whom I have considered to be family since our first holiday season together. I could give each of them the world and still not cover the necessary gratuity to repay them and yet, the brevity of that statement serves no justice to their importance.

My friends and coworkers, past and present, have given me great memories, genius insight, and the interpersonal relationships essential to maintain sanity throughout the course of my education. Of those exceptional people, I want to extend individual thanks to my advisor and friend, Dr. Jeff Volz, as well as my committee members: Dr. Royce Floyd and Dr. Scott Harvey. Also, I must give credit to Jon Drury, (Dr.) Cameron Murray, Mike Schmitz, Trevor Looney, Raina Coleman, Corey Wirkman, Derek Garcia, my brother Josh Choate, and other fellow graduate researchers for assisting with this project.

Lastly, I want to thank the Oklahoma Department of Transportation, the University of Oklahoma, Dolese Bros Co., and the Tier 1 University Transportation Center at Missouri University of Science and Technology for providing the means for this research to reach fruition. Without the commitment of these institutions to the continual research and development of structural technologies, countless projects and ideas for innovation would be left in the dark.

Table of Contents

Acknowledgements ..... **iv**

Table of Contents ..... **vi**

List of Tables ..... **x**

List of Figures ..... **xi**

Abstract ..... **xvi**

Chapter 1: Introduction **1**

1.1 Background **1**

1.2 Objectives and Scope of Work **6**

1.3 Research Plan **7**

1.4 Outline **8**

Chapter 2: Literature Review **10**

2.1 Different Types of Repair **10**

2.2 Repair Versus Replacement **12**

2.3 Repair by Material Replacement **15**

2.4 Removal of Damaged Material **18**

Chapter 3: Previous FR-SCC Research & Development **20**

3.1 Program Outline **20**

3.1.1 Scope of Research *20*

3.1.2 Experimental Procedure *21*

3.2 Results & Conclusions **25**

3.2.1 Small Scale Testing & Material Properties *25*

3.2.2 Large Scale Testing *27*

3.2.3 Results, Findings, & Conclusions *29*

Chapter 4: Initial Testing of AASHTO Girder **30**

4.1 Program Outline **30**

4.1.1 Scope of Research *30*

4.1.2 Research Specimen Description *31*

4.2 Testing of AASHTO Type II Girder **32**

4.2.1 Test Preparation of Girder C *32*

4.2.2 Loading Conditions *34*

4.2.3 South End Test (C1) *35*

4.2.4 North End Test (C2) *38*

4.3 Results & Conclusions **40**

4.3.1 Material Testing Results *40*

4.3.2 Load-Deflection Test Results *41*

Chapter 5: Repair of AASHTO Girder **44**

5.1 Core-Sampled Web Repair **44**

5.1.1 Extent of Damage & Concrete Removal *44*

5.1.2 Formwork Design & Construction *45*

5.1.3 Repair of Internal Reinforcing *47*

5.1.4 Placing the Repair Concrete *48*

5.2 Repair Mix Design Modifications **52**

5.3 South End Repair **54**

5.3.1 Extent of Damage & Concrete Removal *54*

5.3.2 Formwork Design & Construction *56*

5.3.3 Repair of Reinforcing *57*

5.3.4 FR-SCC Monitoring Formwork Additions *63*

5.3.5 Placing the Repair Concrete *65*

5.3.6 Post-Tensioning the Repaired Section *67*

5.4 North End Repair 72

5.4.1 Extent of Damage & Concrete Removal *72*

5.4.2 Formwork Design & Construction *74*

5.4.3 Repair of Girder Reinforcing *75*

5.4.4 Placing the Girder Repair Concrete *83*

5.4.5 Repair of Deck Reinforcing *84*

5.4.6 Placing the Deck Repair Concrete *85*

Chapter 6: Repaired Girder Testing & Results 87

6.1 South End Testing 87

6.1.1 Test Arrangement *87*

6.1.2 Testing Procedure *93*

6.1.3 Results *95*

6.2 North End Testing 96

6.2.1 Test Arrangement *96*

6.2.2 Testing Procedure *97*

6.2.3 Results *100*

6.3 Summary of Results 102

6.3.1 Material Testing Results *102*

6.3.2 Load-Deflection Test Results *103*

Chapter 7: Comparative Analysis, Conclusions, & Recommendations. 105

7.1 Comparative Analysis of Testing 105

7.1.1 South End & Test "C1" *105*

7.1.2 North End & Test "C2" *110*

7.2 Conclusions **115**

7.2.1 Material Properties *115*

7.2.2 Performance of the Repaired Girder *116*

7.3 Recommendations **120**

7.3.1 Application Recommendations *120*

7.3.2 Continued FR-SCC Development Recommendations *121*

Appendix A – Girder Survey Data **125**

Appendix B – Photos of Concrete Removal **130**

Appendix C – Photos of Internal Reinforcing Repair **133**

Appendix D – Supplemental Repair Photos **137**

List of Tables

Table 3.1 15% Komponent Mix Design Properties 21

Table 3.2 15% Komponent Mix Design Proportions 21

Table 3.3 Material Properties for 15% Komponent Mix 26

Table 3.4 Small-Scale Comparative Data 27

Table 3.5 Table 3.5 Full-Scale Beam Testing Comparative Data 28

Table 4.1 Testing Results for Girder C 43

Table 5.1 FR-SCC Mix Design Specifications 53

Table 5.2 FR-SCC Mix Design Proportions, Saturated, Surface-Dry 53

Table 6.1 Repair Material Strength Data 102

Table 6.2 Testing Results for Repaired Girder 104

Table 7.1 South End Comparative Test Results 109

Table 7.2 North End Comparative Test Results 114

Table 7.3 Comparative Girder Concrete Compressive Strengths 116

List of Figures

Figure 1.1 Impact Damaged, Prestressed Concrete Bridge 2

Figure 1.2 Impact Damage Replacement Project in 2017 4

Figure 2.1 University of Minnesota Shotcrete Repair Project 13

Figure 2.2 Rockville Road Bridge Damage 14

Figure 3.1 Large-Scale Specimen Reinforcing Schematic 23

Figure 3.2 Repair Beam After Control Concrete & Before FR-SCC 24

Figure 3.3 Three Finished FR-SCC Repair Beams 24

Figure 3.4 Full-Scale Beam Loading Diagram 25

Figure 3.5 Full-Scale Beam Testing Load vs. Deflection Plots 28

Figure 4.1 Girder "C" Location in Original I-244, Arkansas River Bridge 32

Figure 4.2 Girder C Cross-Sectional Dimensions & Reinforcing Diagram at Midspan 33

Figure 4.3 Test C1 Support Conditions (West View) 35

Figure 4.4 Test C2 Support Conditions (West View) 35

Figure 4.5 Shear & Horizontal Cracking in the Bottom Bell 37

Figure 4.6 Deck Compressive Failure & Wearing Layer Delamination 37

Figure 4.7 East Elevation of Damage Received During Test C1 37

Figure 4.8 Cracking During Test C2 39

Figure 4.9 Buckled, Longitudinal No. 8 Reinforcing Bar in the Top Bell of the Girder 39

Figure 4.10 West Elevation of Damage Received During Test C2 40

Figure 4.11 Load vs. Deflection Plot for Test C1 42

Figure 4.12 Load vs. Deflection Plot for Test C2 42

Figure 5.1 West Elevation of Core-Sampled Web Section 45

Figure 5.2 Assembled Formwork, Core-Sampled Web Repair 47

Figure 5.3 Core-Sampled Web Replacement Reinforcing 48

Figure 5.4 Mix Materials Chilled with Ice 49

Figure 5.5 Extent of Flow for First Pour of Core-Sampled Web 50

Figure 5.6 Core-Sampled Finished Repair (Without Mortar Patch) 52

Figure 5.7 South End Damage From Original Testing 55

Figure 5.8 South End With Damaged Concrete Removed 55

Figure 5.9 South End Formwork SketchUp Design 57

Figure 5.10 Assembled Post-Tensioning Splice Chucks 59

Figure 5.11 Splice Chuck Assembly for Existing Strand 60

Figure 5.12 Post-Tensioning, Grease-and-Sleeve Arrangement 60

Figure 5.13 Fully Installed Post-Tensioning with Partial Formwork 61

Figure 5.14 Bursting Steel for Post-Tensioning 63

Figure 5.15 South End Repair Concrete Flow 64

Figure 5.16 Observation Window for Monitoring Flow and View Through the Window 65

Figure 5.17 South End Repair with Forms Removed 67

Figure 5.18 Anchor Plates After Casting the South End Repair 69

Figure 5.19 Damaged Area After Removal of Anchor Plate 69

Figure 5.20 Post-Tensioning Stressing Order 71

Figure 5.21 Post-Tensioning Strand Stressing 71

Figure 5.22 North End Damage from Original Testing 73

Figure 5.23 Further Damaged Concrete Uncovered During Demolition 73

Figure 5.24 North End with Damaged Concrete Removed and Loose, Existing Reinforcing Steel 74

Figure 5.25 North End Formwork SketchUp Design (West Side) 75

Figure 5.26 Original ODOT Reinforcing Diagram for Girder 77

Figure 5.27 North Boundary of North End Repair 78

Figure 5.28 ODOT Typical Deck Reinforcing Diagram 78

Figure 5.29 Original Deck Reinforcement with Partial Concrete Demo 79

Figure 5.30 Prestressing Tendons in Compression 80

Figure 5.31 Internal Reinforcing SketchUp Model 81

Figure 5.32 North End Girder Internal Reinforcing 82

Figure 5.33 Roughened Surface of North End Girder Portion 84

Figure 5.34 Deck Reinforcing of North Repair 85

Figure 5.35 West Side of Completed North End Repair 86

Figure 6.1 South End Repair Section Before Testing 88

Figure 6.2 South End Test Support Conditions (West View) 89

Figure 6.3 Load Cell Arrangement 90

Figure 6.4 Wire Potentiometers for South End Test 92

Figure 6.5 Laser Level Deflection Base Measurement 92

Figure 6.6 Crack Width of Repair Interface 94

Figure 6.7 Extent of Damage for South End Repair 94

Figure 6.8 South End Test at Maximum Deflection 95

Figure 6.9 North End Test Support Conditions (West View) 96

Figure 6.10 North End Test Instrumentation 97

Figure 6.11 First Cracks in the Repair Zone 99

Figure 6.12 Shear-Bond Cracking in North Repair 99

Figure 6.13 Delamination of Wearing Layer During Repair Testing..... 100

Figure 6.14 Post-Testing West Elevation of North End 101

Figure 6.15 North End Test at Maximum Deflection..... 101

Figure 6.16 Load-Deflection Plot South End Repair Test..... 103

Figure 6.17 Load-Deflection Plot North End Repair Test..... 104

Figure 7.1 First Cracks For South End Repair Beam Test; First Cracks For Murray's "C1" Testing 108

Figure 7.2 Load vs. Deflection Plot of Original and Repair Testing of South End of Girder..... 110

Figure 7.3 First Cracks for Murray's North End Testing 112

Figure 7.4 North End Shear Plane Discovered Mid-Demolition..... 113

Figure 7.5 Load vs. Deflection Plot of Original and Repair Testing of North End of Girder..... 114

Figure A.1 Deck Survey Plot From Initial Testing..... 126

Figure A.2 East Elevation Survey From Initial Testing 126

Figure A.3 West Elevation Survey From Initial Testing..... 126

Figure A.4 West Photographic Elevation From Initial Testing..... 127

Figure A.5 West Photographic Elevation From Repair Testing..... 127

Figure A.6 Enlarged West Photographic Elevation From Initial Testing (North End)..... 128

Figure A.7 Enlarged West Photographic Elevation From Initial Testing (South End)..... 128

Figure A.8 Enlarged West Photographic Elevation From Repair Testing (North End)..... 129

Figure A.9 Enlarged West Photographic Elevation From Repair Testing (South End)..... 129

Figure B.1 Loose Concrete Removed From South End With Hammer 131

Figure B.2 One-Inch Boundary Line Cut With Hand Grinder (South End)..... 131

Figure B.3 North End Bottom Bell & Loose Concrete Removal 132

Figure B.4 Removal of Deck Concrete Using an Impact Hammer 132

Figure C.1 Coupler Housing Construction 134

Figure C.2 Post-Tensioning Anchorage Installed to Formwork With Insulating Foam to Seal the Backside..... 134

Figure C.3 Bent Longitudinal Reinforcing of North End Repair 135

Figure C.4 Turnbuckle Splices for North End Straight Strands 136

Figure D.1 Post-Tensioning Anchor Head..... 138

Figure D.2 Adding Cementitious Material During the Mixing Process 138

Figure D.3 Adding the FR-SCC Repair Material to the South End..... 139

Figure D.4 Slump Flow Test Results of FR-SCC..... 139

Abstract

In 2017, the American Society of Civil Engineers released a report card stating that, of the 614,387 bridges in the United States, nearly 40% are past their design life. Within a few months of the report, the U.S. Department of Transportation posted that over 16% of the nation's bridges are in "poor" or "structurally deficient" condition. With the growing awareness for the current condition of the United States' infrastructure, the FHWA has allocated tens of billions of dollars towards the repair and improvement of bridge and highway infrastructure every year and yet, the current, subpar status is retained. Concrete structures account for almost half of the nation's bridges and to fix an extensively damaged concrete bridge girder, it is common practice to replace the entire member or perform multipart repairs. Either of these options are very costly and can take several months to complete.

This study serves as a continuation of two other research projects; one of which tested an AASHTO bridge girder, the other featured the development of fiber-reinforced, self-consolidating concrete (FR-SCC) as a repair material. The AASHTO, prestressed concrete girder used in the previous study is the subject of repair and repair testing for this research. The girder had been donated by the Oklahoma Department of Transportation after being retired from service and brought into the lab to be tested until failure to acquire its capacities. The state of the girder was documented photographically and through computer-aided design software. Upon completion of the surveying, the girder was repaired using the

previously developed FR-SCC as a replacing, repair material. This repair method requires all damaged concrete to be removed from the girder and any internal reinforcing to be repaired or replaced, as needed. Since the girder is prestressed, the original stress transferred from the strands was reapplied by existing tensioning methods, such as internal splicing. The repair material was cast such that the original shape of the girder was retained, thus maintaining the same aesthetics and geometric properties. Once the concrete had cured and the strand stress reapplied, the girder was tested again to obtain comparable results to the original testing. By analyzing the data from the initial testing and the repair testing, a practical conclusion for the plausibility of FR-SCC implementation as a repair technique was ascertained.

The aim of this study was to repair the girder with FR-SCC and develop a comparison of its capacities before and after repair. The repair material used for each repair yielded a comparable compressive strength to that of the existing concrete in both the girder and the composite deck, while also retaining the necessary workability properties to fully fill the repair zones. When testing the repaired girder, the failure mechanisms from the initial, pre-repaired testing were mitigated and the repair sections acted cohesively with the existing girder portions. Despite the limited extent of the repair zones, the girder was able to sustain over three-quarters of the maximum load from its initial testing. The FR-SCC displayed comparable fresh and mechanical properties to that of existing self-consolidating concretes used for prestressed concrete members.

Chapter 1: Introduction

1.1 Background

In 2017, the American Society of Civil Engineers (ASCE) released a report card that graded the current status of the United States' infrastructure as "C+." Within this report, ASCE found that of the 614,387 bridges in service, just over 9% of these bridges are deemed "structurally deficient," which amounts to one of every eleven bridges. It was noted in the report that the current amount of these structurally deficient bridges has decreased over the past decade, although, almost 40% of the nation's bridges are at or beyond their service life (ASCE, 2017).

The U.S. Department of Transportation released in February of 2018 a detailed table counting the number of bridges based on their condition. The total in the nation was 614,978 and, by their count, over 16% of the bridges were in "poor" condition or are "structurally deficient" (FHWA, 2017). Bridges reach this state by collecting damage over their service life. For concrete bridges, the more common means of obtaining this damage is by weather or chemical erosion, overloading or fatigue, and impact damage. Weathering and chemical erosion deteriorates the concrete and, over time, can wear away the protective concrete cover for the internal reinforcing. The capacity of the member is reduced as the concrete is worn away, but when the internal reinforcing becomes exposed, the corrosion of the section is accelerated. This is often the cause for deterioration of concrete structures (Guettala, 2006). Overloading and fatigue is more common in

bridges whose life span has exceeded the intended service life of the structure or have been subject of an extreme loading condition. Alternatively, impact damage occurs as a result of an object, often a vehicle, striking the structure. The result of an impact damage is unique in that it is often instantaneous, and the damage resembles an explosive failure, which is exemplified in Figure 1.1.

Figure 1.1 Impact Damaged, Prestressed Concrete Bridge (Greenizan, 2017)

The deteriorated state of the country's current infrastructure has been gaining more attention every day, especially with public awareness and scrutiny for government spending. The FHWA allocated $60 billion towards this issue in 2010 alone and every year they repeatedly put tens of billions of dollars into fixing bridges and highways (USDOT, 2014). In more recent years, the budget for bridge and highway repairs has grown by almost 65% from 2006 to 2016. Yet, it is still not enough to raise the infrastructure grade. ASCE estimates that the cost to bring all bridges up to the current standards at an additional $123 billion on top

of the currently allotted amount (ASCE, 2017). Moreover, in 2013, the Federal Highway Administration (FHWA) released that more than half of the bridges in the United States are constructed of either conventionally reinforced or prestressed concrete (NACE, 2016).

When these bridges face structural issues with their superstructure, often the member in question is replaced rather than repaired, like the 2017 Rockville Road Bridge project in Indiana. This overpass was struck by a mobile car-crusher that severely damaged four of the bridges fourteen girders. Since the bridge crossed a busy interstate highway, fixing the damaged structure was of high priority and the project turnaround was expedited. The solution was to remove the four damaged girders and deck then replace them with a new structure. Figure 1.2 shows the repair project at different points in the process. The Indiana Department of Transportation estimated the total cost of the project from impact to opening to be beyond $1.2 million (INDOT, 2017). Repairs can offer a more desirable economic solution when compared to alternatives such as replacement and implementing additional structural components.

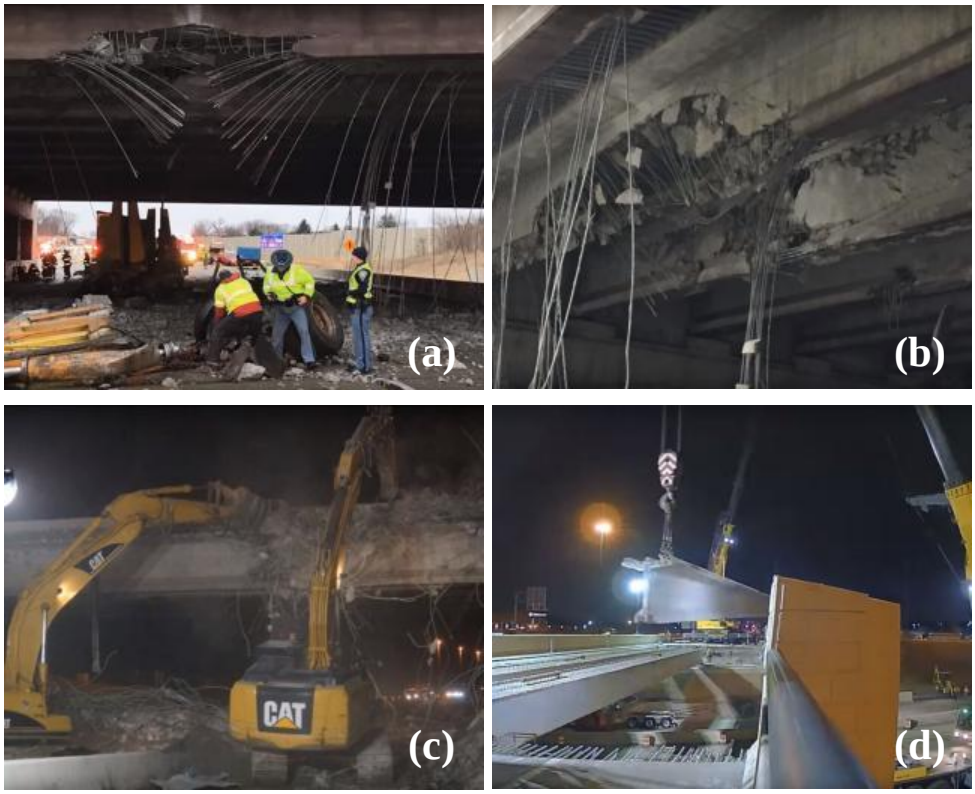

Figure 1.2 Impact Damage Replacement Project in 2017; (a) Initial Impact Cleanup; (b) Damage to Interior Girders; (c) Damaged Girder Removal; (d) Installation of Replacment Superstructure (INDOT, 2017)

For prestressed applications, self-consolidating concrete has inherent properties that make it an ideal repair material. Prestressed concrete practices become preferential for larger spanning concrete girders of which, if conventionally reinforced, may not be able to support their self-weight, let alone any additional load. However, a consequence of using prestressing to accompany these larger spans and larger loads, is the necessity for higher strength concrete. High strength, i.e. high performance, concrete is better suited to handle the higher internal stresses induced by larger spans and the internal prestressing forces. Other considerations when using prestressed applications is the bond between the

concrete and the prestressing tendons and the length needed to fully transfer stresses from the reinforcing tendons and the concrete. Self-consolidating concrete (SCC), however, has a very low viscosity as compared to conventional concrete, allowing it to flow under its own weight and to form to rough, uneven surfaces, such as tendons, without the need for mechanical vibrators. This in turn allows the concrete to be used in areas of high congestion from the internal components. In addition, it is currently common practice for prestressed concrete fabricators to incorporate the use of SCC in the production for the aforementioned reasons. Therefore, using a repair material that is similar to that which was originally cast for a damaged, structural component is rational.

One drawback to SCC is that, like conventional concrete, it is susceptible to shrinkage. When applying new SCC to existing, aged concrete, the new concrete will undergo shrinkage cracking and often debond itself from the aged concrete at the interfacial boundary between the two concretes. To counter this shrinkage, fibers and shrinkage-compensating cement is added. Fibers help to reduce drying shrinkage and control cracking propagation while the shrinkage-compensating cement is an expansive agent. When paired together, an increase in shrinkage resistance occurs; more so than just using one without the other. It has also been found that when the two are implemented, the performance of the fiber-reinforced, self-consolidating concrete (FR-SCC) in its cured, hardened state has the ability to achieve upwards of ten times the overall performance of

conventional SCC when considering properties such as toughness, stiffness, and structural resilience as well as resistance from shrinkage (Kassimi, 2013).

1.2 Objectives and Scope of Work

There are two studies that are a precursor to this research, one of which involves the development of the FR-SCC used as the repair material hereon, the second encompasses the original testing for a retired, AASHTO Type II bridge girder with composite deck. The primary task for this research was to evaluate the practical application of the previously designed FR-SCC as a repair material as well as its effects on the structural performance of the bridge girder when repaired. With the aim of paralleling the initial testing of the girder, the capacity of the girder for each repair test will be analyzed and evaluated in comparison to the originally tested capacities. The anticipated outcome of the study was whether or not the FR-SCC was a realistic solution for industry and if the resulting repair would permit comparable loading behavior to the original testing.

In order to achieve the aforementioned research goals, the following scope of work was put into place:

- research and review pertinent literature,
- design a research strategy,
- survey and record the damage from the initial testing,
- set extent of repair based on survey information,
- demolish and remove damaged concrete within repair zone,

- repair and/or replace any damaged internal reinforcing,
- design and build formwork for FR-SCC replacement,
- cast repair zone with FR-SCC,
- test the repaired girder to failure and record testing data,
- analyze the test data and findings and develop a comparative analysis between the initial testing and repair testing,
- ascertain conclusions from comparative analysis and build a list of recommendations,
- then, compile the documented information of the study into a thesis.

1.3 Research Plan

The practical application of and structural performance of FR-SCC as a repair material for damaged, concrete structural members was evaluated for this study. The FR-SCC mix design was specifically developed for the purpose of repairing structural concrete specimens and was the focus for a previous study centered on the effects of direct replacement of a percentage of the cementitious material with a shrinkage compensating cement. A retired AASHTO Type II bridge girder, donated by the Oklahoma Department of Transportation (ODOT), was initially tested to failure in a study that was executed in advance of this research. The girder and its initial test data were reallocated for the use in this investigation upon completion of its original study.

When conducting the evaluation of the repair application and ensuing testing performance, small-scale testing and large-scale testing was utilized. Small-scale testing was limited to compressive strength testing of the repair material which was based on ASTM C39/C39M – 17a *Standard Test Method for Compressive Strength of Cylindrical Concrete Specimens*. For the large-scale side of the program, the evaluation encompassed a single girder with three distinct repair zones near the load points for testing. When testing the repaired girder, it was loaded in a way that each end of the girder was tested without influencing the other so that a total of two repair tests were performed.

1.4 Outline

Incorporated in this document are a total of seven chapters and appendices. This chapter, Chapter 1, provides a short explanation why repair is important, why FR-SCC was chosen, as well as the objective and scope of this research. A literature review of current repair techniques, potential approaches, and other research relating to this study are given in Chapter 2. Chapter 3 provides an overview of the research and development that led to the development to the FR-SCC used in this program. The history of the research specimen that was repaired is presented in Chapter 4. Chapter 5 details the repair process, and the repair testing is discussed in Chapter 6. A comparative analysis, the resulting conclusions, and recommendations are offered in Chapter 7. The appendices

contain supplemental photographs of the girder throughout different stages of the repair process.

Chapter 2: Literature Review

2.1 Different Types of Repair

One of the most commonly damaged structural members of a bridge are the girders, which are often the recipient to various damaging actions, such as chemical and weathering deterioration, overloading or fatigue, impact damage, etc. When restoring a bridge girder it is crucial to develop and evaluate all potential options. There are many potential solutions to addressing a damaged structural member; the first of which is to repair the member. Repairs are implemented as the member is in place, without significant impact on traffic and is often a more economical choice. There is a long list of repair methods that vary depending on the degree of damage that a concrete member has been subjected to, e.g. cracking or partial section loss. Some of the common methods for more detrimental damage to a member are: conventional placement of normal, high-strength, rapid-set, or fiber-reinforced concrete, jacketing, preplaced-aggregate concrete, and applying shotcrete.

Conventional placement involves casting new concrete in place of the existing, damaged concrete. This approach is viable for damaged concrete that extends well into the existing section. Some considerations when using this method are the effects of shrinkage in the replacing material and that it is not recommended for areas subjected to further corrosion. Further considerations include: preparing the face of the existing concrete to create adequate bond to the repair material and to ensure proper consolidation and filling of the repair zone.

Similar to conventional placement, jacketing is casting new concrete around the existing section and can be made from steel, wood, or concrete. The shortcomings of conventional concrete apply for jacketing as well. Preplaced-aggregate concrete, also known as pressure grouting, is a form of conventional placement that involves filling the repair zone with large aggregates then pumping a grout mixture into the forms to fill the voids between the large aggregates and in tight spaces (Woodson, 2009; Zorbell, 1996). Shotcrete is the pneumatic application of concrete that, because its high-velocity application, results in "excellent bond" to the existing structure (Woodson, 2009). Although, shotcrete, like jacketing, is typically a superficial repair that is usually limited by the thickness of its application.

Another alternative for regaining the capacity of a section is by applying fiber-reinforced polymers (FRP) to the surface of the member. FRP composites are comprised of two main components: the fibers, which are usually glass, carbon, or steel, and the binding, polymer resin. They can be attached to the structure as a preformed panel or applied directly to the member. Direct application involves the preparation of the structural surface for the wet lay-up of fiber sheets with resin. This method is proven effective for flexural and shear strengthening as well as confinement and ductility enhancement for columns. However, FRP systems can only be applied to the surface of a member after the damage has been mitigated, especially if corrosive elements were the cause. The interfacial bond between the concrete and FRP is "critical" to the durability of the

system and the strength gain of the system (Alkhrdaji, 2015). The debonding of the FRP occurs when the strain in the adhesive surpasses its own capacity and the FRP detaches from the concrete. In practice, it is preferred to keep the impact of the repair on traffic at a minimum, so preformed FRP panels are preferred for in situ applications. The issue with this is that preformed panels only come in certain shapes (Kasan, 2012). One advantage of the implementation of FRP is that it effectively lowers the rate of deterioration by corrosion by chemicals and natural elements. This, in addition to its structural advantages, provides for an increased durability of a member, which can be used in conjunction with a conventional repair method and lowers the costs of maintaining the structure (Nossoni and Harichandran, 2010).

2.2 Repair Versus Replacement

In a study conducted by the University of Minnesota, severely deteriorated bridge girders were repaired, removed, and tested along with identical, undamaged girders from the same bridge. The corroded girders were repaired in situ by adding reinforcement around the damage, then applying shotcrete as shown in Figure 2.1. All four girders were extracted (two repaired and two undamaged, unrepaired), then taken to the University of Minnesota for shear testing. Testing revealed that the repair was able to restore the capacity of the damaged girders to that of the undamaged, unrepaired girders. Moreover, the repair was able to be performed without affecting traffic and at a significantly

lower cost than replacement at about $5,500 and $12,500 for each repair. This "box end" repair method was concluded as being a viable repair method for deteriorated girder ends (Shield, 2018). However, the report did not provide any insight on its ability to restore girders at other locations along the span of the girder or its effect on girders with more extensive damage throughout the section.

Figure 2.1 University of Minnesota Shotcrete Repair Project; (a) Added Repair Reinforcing; (b) Shotcrete Application; (c) Completed In Situ Repair (Shield, 2018)

In 2017, the Rockville Road bridge in Indianapolis had to have a portion of the bridge replaced. This job required immediate attention to address the structural integrity of an impact stricken superstructure. The impact, delivered by

a mobile car-crusher traveling on the interstate below the bridge, caused four of the bridge's 125-foot-long girders to suffer catastrophic localized damage. Due to the necessity of the bridge and the high volume of traffic, the project was dubbed a "high-priority bridge repair." The existing four damaged girders and the deck they supported were removed, replacement girders were installed, and a new deck was cast in place of the old. The project lasted nearly five months and the total project cost was reported to exceed $1.2 million in cost from initial impact to reopening (INDOT, 2017). When comparing the costs between this replacement and the previously mentioned shotcrete repair, the replacement was astronomically higher than that of the repair. This is true for nearly all repairs when compared to replacements. Figure 2.2 illustrates the destruction from the impact of the Rockville Road bridge.

Figure 2.2 Rockville Road Bridge Damage (INDOT, 2017)

2.3 Repair by Material Replacement

When considering the repair of a prestressed concrete girder or any prestressed concrete member, there are two stages to properly restore the section: repair of the reinforcement and replacement of the concrete. The former, reinforcing repair, should be the first to be addressed. Robert Zobel (1996) studied two methods of strand repair for prestressed concrete girders: internal splices and external post-tensioning. He found both methods could be sensitive to fatigue loads because the techniques that were analyzed all included wedges in the anchorage zones. and suggested these methods only be used to provide "precompression" for the repair area. Also, these repairs were found to be a way to extend the life of the structure instead of actually restoring the member's original strength. External post-tensioning is done by prestressing tendons or high strength steel bars that are attached to the sides through a steel arrangement that is bolted to the girder. By forcing the repair zone into compression, this method provides for a more durable repair despite having a lower aesthetic value. Unlike the previous method, internal splicing would not put the surrounding concrete into compression immediately, but by using a combination of splicing and prestressing preload applications, the stress in the strands could be restored, then the patching material can be added (Zobel, 1996).

Once tensioning and reinforcement is properly placed or exchanged, the repair concrete can be added. The replacment, repair concrete needs to fully fill the repair zone despite any obstacles in the zone, such as internal reinforcing, and

bond with the existing material. The effectiveness of a repair to restore and extend the service life of a structure is dependent on its individual mechanical and workability properties as well as its compatibility and capacity to maintain bond with the existing structure. In the past, achieving a concrete mixture that possessed the correct hardened properties meant high labor costs to ensure that the material was fully consolidated and placed within its set time. A concrete with high flow properties while still maintaining a consistent mixture with high-strength mechanical properties is necessary for a repair material (Kassimi, 2013).

Self-consolidating concrete (SCC) is an optimal choice for replacement concrete because it retains these unique capabilities. A strong bond to the existing concrete and internal reinforcement is essential to the performance of the member. SCC has better bond stresses due to its high-flowing, non-segregating nature and its ability to properly fill formwork, areas around reinforcement, and rough surfaces of existing concrete with little to no mechanical consolidation (Long et al., 2013). This ability to sustain high bond strengths is owed to the low water to cement ratios of SCC. This high cement content is accomplished by the inclusion of viscosity-modifying admixtures (VMA), high-range water reducers (HRWR), and smaller course aggregates (Long and Feng, 2014). There are other available materials that can improve additional aspects of SCC, like supplementary cementitious materials (SCM) that provide for higher compressive strengths as compared to traditional, normal strength concrete. SCC also has a comparable

modulus of elasticity and flexural strengths to other high-performance concretes of similar mixtures (Long et al., 2013).

One major drawback to SCC is that, in many cases, it is susceptible to shrinkage cracking during the curing process. Addressing this issue can be handled in a number of ways, the first being to introduce fibers to the mix design. The fibers help to control the cracking behavior by absorbing the energy that causes cracks to form. However, there is a balance to how many fibers can be added to the concrete in order to maintain its high workability. If this ratio is optimized, then the resulting fiber-reinforced, self-consolidating concrete (FR-SCC) can achieve higher tensile strengths and increased ductility when compared to mixes without fibers. Alternatively, shrinkage-compensating admixtures (SCA) or expansive agents (EA) can be added to the concrete to reduce the effects of shrinkage. In a study performed by Kassimi in 2013, the effects of adding fibers, SCAs, and/or EAs to SCC were evaluated for the purpose of repair material development. Some of the results were that the EA, a powder-based material, was better able to resist shrinkage cracking than SCA, a liquid-based material, and when including EA in FR-SCC, that mix was the best solution for alleviating shrinkage cracking as well as being the most efficient in terms of performance to cost relations (Kassimi, 2013).

2.4 Removal of Damaged Material

Before the actual repair can take place, loose or structurally deficient concrete must be removed. As stated in previous sections, the bond between the repair material and existing materials is imperative to the success of the anticipated capacity restoration. Thus, the removal must be done in a manner that the replacement concrete will be able to adhere to structurally sound, existing concrete. Removing concrete can be done in a number of different ways, some of the more common approaches are by blasting, crushing, cutting, impacting, milling, and presplitting.

As the name implies, blasting implements explosives to remove large sections of concrete. Crushing is one of the more portable methods for removing concrete. This method utilizes hydraulic jaws to remove the concrete. The method comprised of fracturing the concrete by striking the surface usually involves a tool such as a jackhammer. Milling is achieved, in most cases by hydromilling, high-velocity water jets that erode the concrete, or by rotary milling. Both techniques are effective, but not realistic due to their tendency to cause more damage than intended. The last concrete removal method, presplitting, involves creating holes in the concrete at specific locations in order to control where cracks propagate. Out of the many different methods to removing concrete, one widely accepted method is to use “handheld impact breakers,” which are especially proficient in demolishing shallower segments of concrete and are highly versatile. Upon completion of the concrete removal, the face of the existing concreate should be

cleaned by compressed air or water. When the repair material is to be applied, the surface should be dry and thin layers of 2 inches or less should implement a bonding agent (Woodson, 2009).

Chapter 3: Previous FR-SCC Research & Development

A portion of this study builds on the preliminary research "Performance of Fiber-Reinforced Self-Consolidating Concrete for Repair of Bridge Sub-Structures" conducted by Cory Wirkman and Dr. Jeffery Volz (2016). By implementing small- and full-scale testing, the study was able to develop and test various characteristics of the proposed fiber-reinforced, self-consolidating concrete (FR-SCC) mix design used in this study, which will be detailed in later chapters. With the aim of completeness, a brief overview of Wirkman's research is presented in this chapter.

3.1 Program Outline

3.1.1 Scope of Research

In Wirkman's investigation, three different concrete mixtures were developed and tested. The constant and baseline for the study was an Oklahoma Department of Transportation (ODOT) Class AA mix that was used to produce several large- and small-scale specimens. This design was compared to two other FR-SCC based mix designs with differing amounts of Komponent®. Being a Type K, shrinkage-compensating, cementitious material, Komponent® is suitable when applying new concrete to preexisting concrete members. These mix designs call for the direct replacement of a percentage of the total cementitious material with Komponent®; in Wirkman's study, this percentage and its structural effects were a primary focus for the development of the repair material. The replacement

percentages evaluated were 10% and 15% of the portland cement with shrinkage-compensating cement. The mix design for the 15% Komponent was chosen as the repair material for the overall study discussed later in this document and its mix design is presented below, in Table 3.1 and Table 3.2. Mix designs for the 10% Komponent replacement and the Class AA control mix are detailed in Wirkman's study (2016).

Table 3.1 15% Komponent Mix Design Properties

Water/Cementitious Material Ratio	0.39
Fly Ash Replacement (by Mass)	30.0%
Komponent Replacement (by Mass)	15.0%
Volume of Fine Aggregate	50.0%
Volume of Fibers	0.5%

Table 3.2 15% Komponent Mix Design Proportions

Type I/II Cement	413.1 lb/yd^3
Class C Fly Ash	224.1 lb/yd^3
Komponent	113.4 lb/yd^3
Water	177.2 lb/yd^3
Fine Aggregate	1401.3 lb/yd^3
Course Aggregate	1223.1 lb/yd^3
MasterFiber MAC Matrix	7.7 lb/yd^3
Air-Entrainer, MB-AE 90	1.1 fl. oz/cwt
HRWR, Glenium 7500	9.0 fl. oz/cwt

3.1.2 Experimental Procedure

Large- and small-scale specimens were constructed then tested to relate the performance of the FR-SCC mixes to the ODOT Class AA mix. Early in the

developmental stages of the repair mixes, several fresh concrete properties were evaluated to ensure the mixes would adhere to the design standards set by Wirkman and Volz for the purpose of their research. Primarily, those standards consisted of parameters that characterized a high-flowing, well-filling, concrete with a similar air content and unit weight to the ODOT Class AA mix. However, the highlight of those standards was a slump flow of 28 inches with no segregation of materials or bleeding of the concrete. The tests for slump flow, unit weight, air content, and a customized flow test intended to evaluate the flow and fill properties of the FR-SCC specifically for the large-scale applications.

The large-scale specimens entailed three separate beams for each mix design: three monolithically cast control beams using the ODOT Class AA mix design, three "repaired" beams with the 10% Komponent FR-SCC mix design in the tension zone, and three "repaired" beams with the 15% Komponent FR-SCC mix in the tension zone. Each of the large-scale specimens measured 14'-0" in length, 18 inches tall, and 12 inches wide with four Grade 60, No. 6, longitudinal, steel reinforcing bars in the tension zone, as shown in Figure 3.1. The non-control beams were cast with the FR-SCC repair mix at the bottom of the specimen. This section of the beam had a depth of 7 inches on one end of the beam and tapered down to 5 inches on the opposite end, thus allowing for a better flow of the repair mix. A conservative shear stirrup spacing was used to guarantee a flexural failure mechanism. Each beam featured two 4 inch fill holes near the ends of the beam

and two 1 inch vent holes near the third points of the beam, both in the control concrete section of the beams.

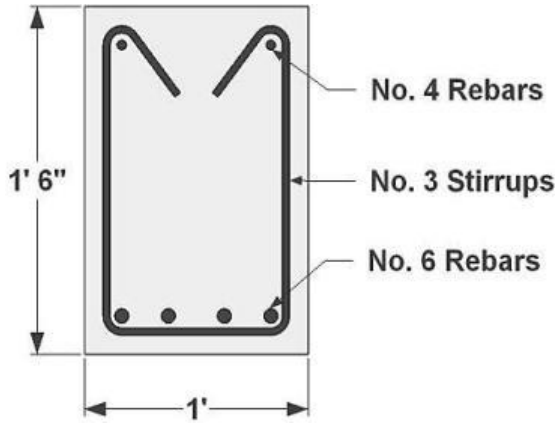

Figure 3.1 Large-Scale Specimen Reinforcing Schematic

In order to test the plausibility of the repair mixes as a true repair solution, the top portions of the non-control beams were originally cast inverted with the control concrete on the bottom. After curing for 28 days, the beams were flipped over so that the repair section was now on the bottom and the control concrete was at the top, then placed back into the forms. This arrangement is shown in Figure 3.2. The FR-SCC mixes were added to the appropriate beams through the fill holes until the mix began to escape through the vent holes, the finished result is shown in Figure 3.3. These beams were allowed to cure for another 28 days before testing. All the large scale beams were tested using a third-point loading method as in Figure 3.4 and the performance was monitored visually and through deflection and strain gauges.

Figure 3.2 Repair Beam After Control Concrete & Before FR-SCC (Wirkman, 2016)

Figure 3.3 Three Finished FR-SCC Repair Beams (Wirkman, 2016)

The small-scale testing incorporated the standard material property testing such as slump/slump flow, unit weight, and air content for fresh concrete. Other material property tests included bond strength, compressive strength, splitting tensile strength, modulus of rupture (MOR), and modulus of elasticity (MOE). For the flexural testing, monolithic MOR prisms as well as composite prisms

were developed with the same material as the full-scale specimens. All tests were conducted in accordance with the appropriate ASTM standards. The small-scale flexural testing utilized a third point loading system, ensuring a constant moment section just as with the full-scale specimen tests. Bond strength testing for the FR-SCC mix designs was based on ASTM C 882, *Standard Test Method for Bond Strength of Epoxy Resin Systems Used With Concrete By Slant Shear* (2013). The specimens used in these tests were 6 inch x 12 inch cylinders with half of the specimen consisting of the FR-SCC mix design.

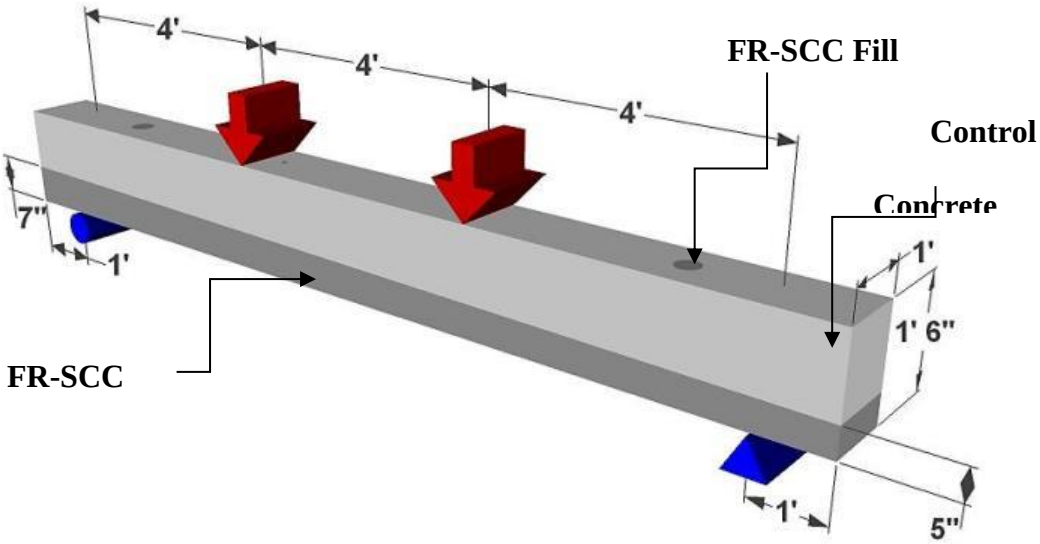

Figure 3.4 Full-Scale Beam Loading Diagram

3.2 Results & Conclusions

3.2.1 Small Scale Testing & Material Properties

Small scale and material property testing results fell within a reasonable tolerance of the target values while exceeding a few of them. The target values for the concrete properties of the repair mixes were a slump flow of 28 inches, an air

content of 6%, and a compressive strength of at least 4000 psi. The results for the 10% Komponent FR-SCC mix yielded a slump flow of 32 inches, 9% for the air content, a compressive strength of 4740 psi, a MOE of 3952 ksi, and a splitting tensile strength of 406 psi, all at an age of 28 days. Results for the 15% Komponent FR-SCC mix design are listed in Table 3.3 and Table 3.4, some of the key values are as follows: a slump flow of 30 inches, 10.5% for the air content, a compressive strength of 6010 psi, a MOE of 4081 ksi, and a splitting tensile strength of 511 psi, all at 28-days.

Table 3.3 Material Properties for 15% Komponent Mix

Properties (Units)	Target Value	Achieved
Slump Flow (inch)	28.0	30.0
Air Content	6.0%	10.5%
Unit Weight (lb/ft^3)	-	138.7
Compressive Strength (28-day, psi)	4000	6010
Splitting Tensile Strength (28-day, psi)	-	511.4
Modulus of Rupture (psi)	-	548.4
Modulus of Elasticity (ksi)	-	4081

Table 3.4 Small-Scale Comparative Data

Strength Test	Control	10% Komp.	15% Komp.
Compressive Strength (28-day, psi)	6740	4740	6010
Splitting Tensile Strength (28-day, psi)	459.1	406.3	511.4
Composite Modulus of Rupture (psi)	-	693.0	693.0
Bond Strength (psi)	-	475.9	569.8

3.2.2 Large Scale Testing

The results of the large-scale testing showed that the repair mixes had ultimate moments that were "statistically equivalent" to the Class AA mixture. All of the experimental ultimate moments were within 5% of the calculated capacities. The cracking moments for the control beams and 10% Komponent mix beams were equivalent to the theoretical values. However, the 15% Komponent mix beams only withstood 81% of the calculated value for the cracking moment. Average values for the three sets of beams tested are shown in Table 3.5 and load versus deflection plots for all nine beams are shown in Figure 3.5. The three sets of beams performed with a consistent load-deflection response for each mix type. Deflections for the control beams were marginally less than the deflections of the repaired beams for both the uncracked and cracked periods of testing. Once the beam loadings reached the point where the steel was beginning to yield, the deflection response for all the beams were nearly identical. Crack propagation and the extent of cracking were virtually the same between all beams and all concrete

types. It was noted, though, that there were a limited number of cracks on the repair beams that did follow the concrete interface for a short distance and then those cracks trended upward, toward the load point.

Table 3.5 Table 3.5 Full-Scale Beam Testing Comparative Data

Mix	Avg. Cracking Load (kips)	Avg. Ultimate Load (kips)	Avg. Cracking Moment (k-ft)	Avg. Ultimate Moment (k-ft)
Contol	17.2	94.2	33	189
10% Komp.	16.9	91.2	33	182
15% Komp.	13.1	90.1	25	180

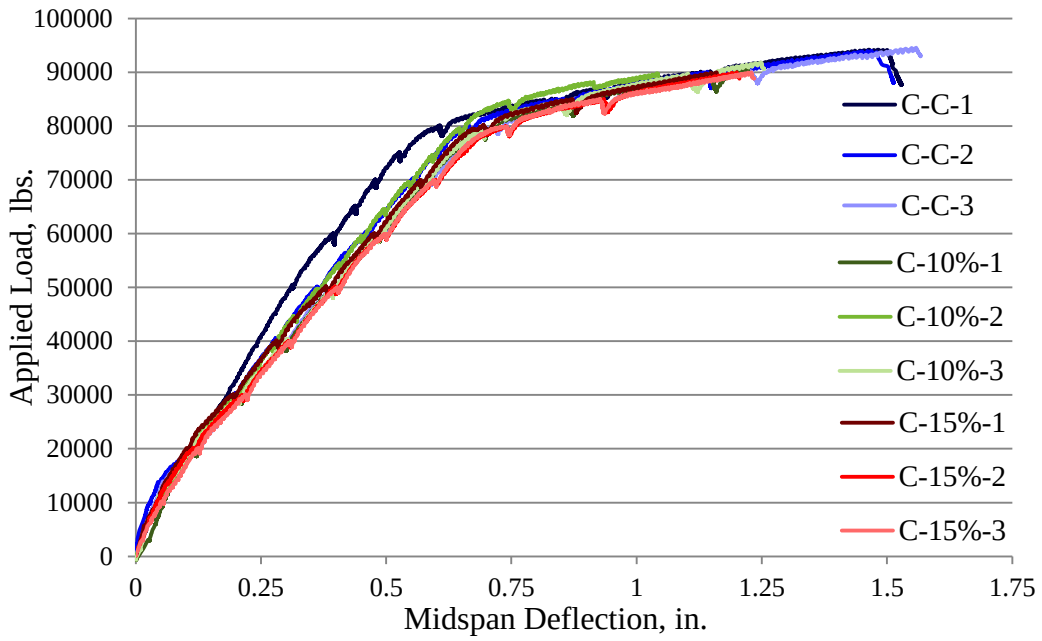

Figure 3.5 Full-Scale Beam Testing Load vs. Deflection Plots

3.2.3 Results, Findings, & Conclusions

On the whole, the testing and performance of the two repair mixes and their cast specimens performed identically to the Class AA mixture. As for the full-scale testing, the two sets of repaired beams withheld similar ultimate moments, had similar load versus deflection plots, and exhibited similar cracking behaviors. Yet, one of the noted differences was that with the dosage increase of Komponent®, there were lower cracking moments values. This was believed to be due to the shrinkage plane along the old and new concrete bond interface. The other major difference, as mentioned previously, was the cracking pattern for the repair mixes where the cracks followed the old and new concrete interface for a small distance before continuing their trend toward the load point. This was interpreted to mean that there was a possibility of debonding or slipping between the repair material and the originally cast concrete. The small-scale specimens revealed that when cast as a monolithic prism, the repair mixes had a marginally lower modulus of rupture when compared to the Class AA prisms. Higher Komponent® replacement levels brought higher bond strengths and it was believed to be owed to the lower shrinkage allowed by the shrinkage-compensating cement.

Chapter 4: Initial Testing of AASHTO Girder

The study on the bridge girder preceding this research was carried out by Cameron Murray, a PhD. student during the following study, and Dr. Royce Floyd at the University of Oklahoma (2017). In partnering with the Oklahoma Department of Transportation (ODOT), Murray was able to perform multiple tests on two retired, prestressed, concrete bridge girders, one of which was used in this overall study as the specimen to be repaired and retested. This chapter details the history of that member and its original testing.

4.1 Program Outline

4.1.1 Scope of Research

In Murray's study, he utilized two AASHTO Type II bridge girders in his research as full-scale test specimens, comparing the test results to values from an Excel spreadsheet developed to analyze the shear capacity. This program took into account several differing analysis approaches, including: AASHTO's 1973 Standard Specifications, the AASHTO modified compression field theory (MCFT) load factor and resistance design (LFRD) using the beta-theta tables from the sixth edition bridge code, the AASHTO MCFT LFRD simplified technique, and the ACI method based on the 2014 version of ACI 318. The assessment of the "residual" shear performance of the retired bridge girders was the intention of the full-scale study in addition to the effects caused by corroded ends, composite decks, and diaphragms.

4.1.2 Research Specimen Description

There were two AASHTO Type II girders utilized in Murray's research, the first was a 32-foot-long girder, denoted as "girder A" and the second was the 46-foot-long girder that was used in this study, labeled "girder C" in Murray's literature. These members were salvaged from an existing bridge in Tulsa, OK, that was to be replaced in 2013. The name connotations originate from the construction drawings provided by the ODOT, where the superstructure of the bridge was supported by six girders designs which were detailed as "beam A" through "beam F," shown in Figure 4.1. One "beam A" and one "beam C" were selected as the two representative samples of the four reinforcing arrangements used for the bridge. ODOT donated the girders with the intention of facilitating full-scale testing as part of research projects from 2014 to 2016 in conjunction with the University of Oklahoma. Originally, the girders were constructed in the 1960's as a part of the eastbound I-244 bridge crossing the Arkansas River just west of downtown Tulsa. Girder C was removed from the structure in September of 2013 with a 3-foot-wide section of the deck and diaphragms at each end and at midspan. When removing the member, the deck was not cut centered on the vertical axis of the girder, thus requiring construction of a 10-inch-wide section of deck that was added later in order to maintain a symmetrical cross-section. (Details on this addition are discussed in Section 4.2.1 Test Preparation of Girder C.) The girders were transported to the University of Oklahoma in October of

2013, and more information related to the transportation of girder C can be found in the dissertation by Murray (2017).

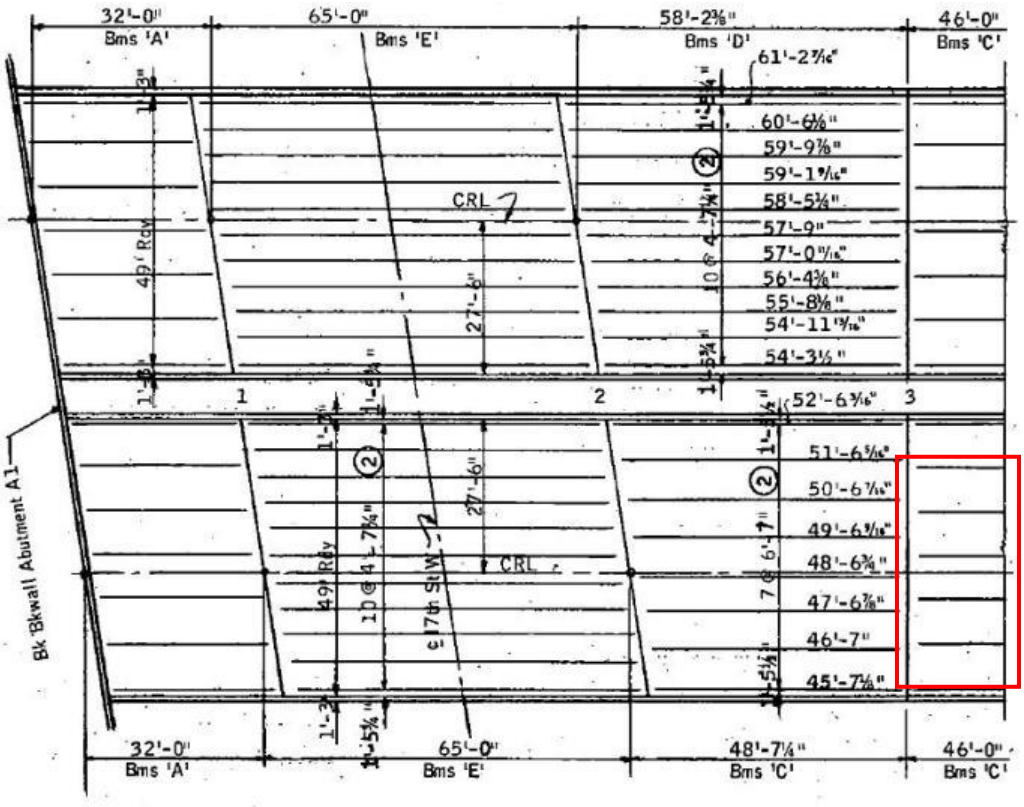

Figure 4.1 Girder "C" Location in Original I-244, Arkansas River Bridge

4.2 Testing of AASHTO Type II Girder

4.2.1 Test Preparation of Girder C

At the University of Oklahoma, Donald G. Fears Structural Engineering Lab, the girder was painted white and a reference grid was marked on the face of the girder on 6" intervals both vertically and horizontally to enhance the visibility of cracks during testing. The aforementioned, 10-inch-wide deck addition was

constructed using a concrete mixture designed to mimic the properties of the existing deck and its design was based on core samples that were taken from the deck portion of girder A. Holes were drilled horizontally into the existing deck at the interface between the supplemental concrete and the existing deck. No. 4 transverse bars were forced into the holes and anchored with epoxy in a manner that left enough of the bar protruding into the deck extension so as to facilitate the carrying of the compressive forces across the interface into the deck extension. Also, four longitudinal reinforcing bars, matching the original deck reinforcing, were placed in the extension, one in each corner of the cross-section. The deck extension along with the reinforcing details are shown in Figure 4.2.

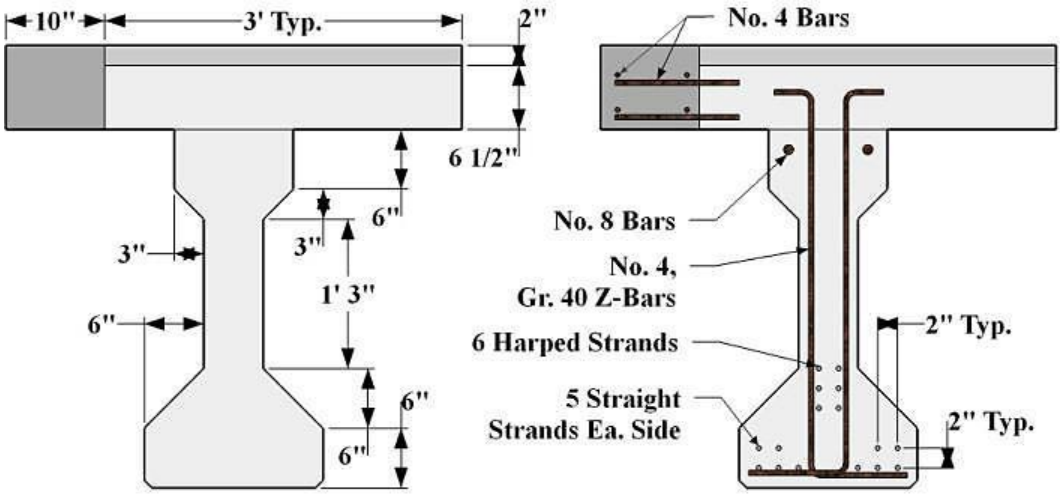

Figure 4.2 Girder C Cross-Sectional Dimensions & Reinforcing Diagram at Midspan

4.2.2 Loading Conditions

The testing regions were defined by *a/d* ratios of 3.0 and 3.83, which were selected in order to observe quarter-point loading behavior with the support conditions chosen based on eliminating the influence of one test region on another. That is to say, the supports were arranged in each test so that both test regions would not be loaded but one would be cantilevered beyond one of the supports. The *a/d* ratios were chosen based on inducing maximum shear stresses in the region of the girder that resides well outside of the discontinuity region. The intention was to achieve an arrangement in which the tested section of the beam would be a minimum distance *d* from the support and from the load point. Additionally, in order to replicate on-site conditions, the supports featured neoprene bearing pads with identical dimensions of those detailed on ODOT's original drawings. The load/support locations for each test are as follows: Murray's first test (C1, shown in Figure 4.3) which coincides with the south end of the girder has a support at the end of the beam, a load point 9 feet from the centerline of the end support, and the second support is centered at 16 feet beyond the load point. The second test (C2, shown in Figure 4.4) conducted on the north end of the girder also had a support at the end with the load point 11.5 feet from the centerline of the end support, then the second support is centered at 16.5 feet from the load point.

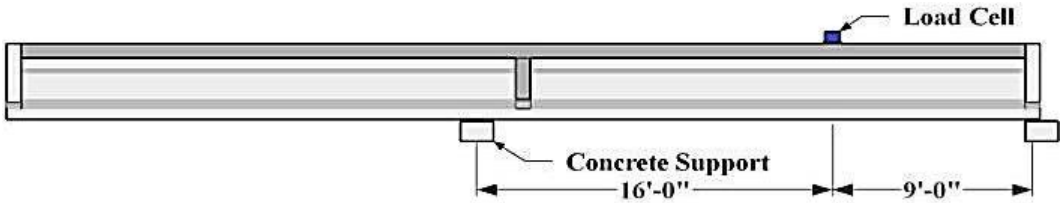

Figure 4.3 Test C1 Support Conditions (West View)

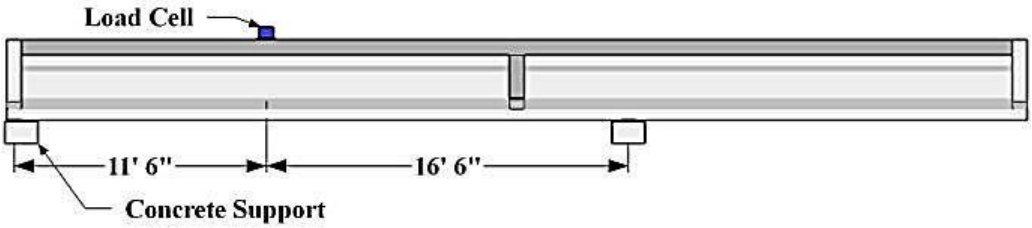

Figure 4.4 Test C2 Support Conditions (West View)

4.2.3 South End Test (C1)

For the testing of Girder C, Murray used linear variable differential transformers (LVDTs) to gauge the strand slippage for all but two of the straight strands along with four LVDTs at the bearing locations to record the vertical deformation of the bearing pads during testing. Wire potentiometers were utilized for deflection at the location of the point load, and several strain gauges, varying in type, were used in multiple locations. No preload was applied for the first test of the girder (C1) and loading increments were kept at 10 kips with the intention of monitoring crack propagation. As these cracks appeared, they would be traced with a black marker for the extent of the crack that would be visible to the naked eye. The end of the trace would then be marked with a perpendicular line signifying the extent of the crack under the current load, then the load would be

recorded next to the perpendicular line. Spalling behavior began at 90 kips of applied load where the girder bears on the southernmost support and continued until the loading reached 110 kips. It was noted that the extent of the corrosion accompanied by the bearing force was causation for cracks formed before testing to reopen and small sections of concrete to spall off the bottom bell of the girder. Web-shear cracking was first recorded at 160 kips of applied load and the initial propagation of flexural cracks were logged at 195 kips. At this load point, cracking in the bottom bell began to progress in a manner that suggests a bond-shear failure was occurring, an example of which is shown in Figure 4.5. This progress continued to 260 kips of load where the cracks were observed to follow the length of the straight strands in the bottom bell. Beyond the 300 kip load increment, the girder began to display signs of plastic deformation. Murray described the performance just before failure as increased deflection per load complemented by further spread of shear cracking in the bottom bell. This shear cracking is believed to be the source for the ultimate failure by contributing to debonding of the prestressing strands leading to compressive failure of the concrete in the deck at an applied load of 318 kips. The compressive failure in the deck led to partial delamination of the 2-inch-thick wearing layer on the topside of the deck, and the result is shown in Figure 4.6. Figure 4.7 shows the full extent of the damaged received during test C1.

Figure 4.5 Shear & Horizontal Cracking in the Bottom Bell

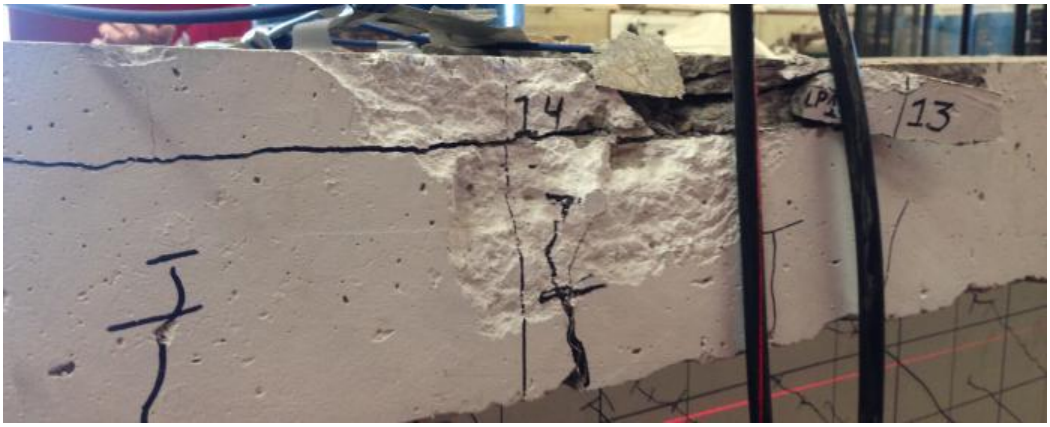

Figure 4.6 Deck Compressive Failure & Wearing Layer Delamination

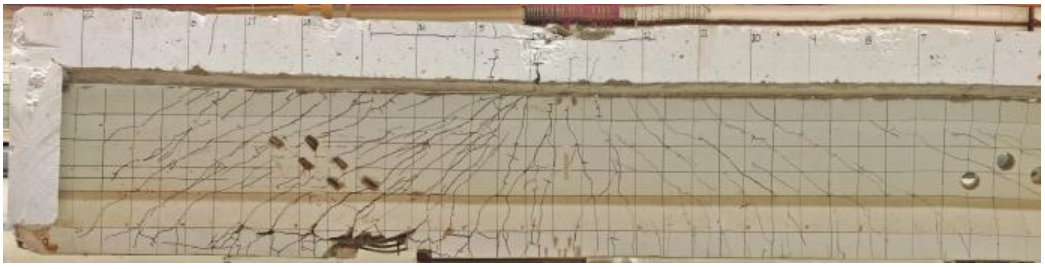

Figure 4.7 East Elevation of Damage Received During Test C1

4.2.4 North End Test (C2)

The second test (C2) featured a loading location at the quarter-span of the original girder length. This location was predetermined to be the critical section for shear, although, with an *a/d* ratio of 3.83, flexural failure was anticipated to be a controlling factor. Cracking was initially recorded at 150 kips of load in the form of web shear cracks at a location approximately 2 feet from the north support. Flexure cracks first propagated at a load of 160 kips and continued to develop until reaching the deck at a load of 190 kips, roughly. Shear cracks in the web started to expand into the bottom bell forming flexure-shear cracks at 195 kips of applied load. A number of these cracks began to traverse laterally, in the direction of the strands as more load was applied, suggesting bond failure along the tendons. Figure 4.8 illustrates the various types of cracking behaviors in test C2. Load was continuously applied until ultimate failure at which the compressive forces in the deck caused the longitudinal steel to buckle (Figure 4.9), the two-inch overlay to delaminate, and the deck itself to buckle. Murray noted this as either a compression-shear failure, which is the result of shear cracks entering the compressive zone leading to failure by compression, or simply a flexural failure. The extent of the damage caused by test C2 is shown in Figure 4.10.

Figure 4.8 Cracking During Test C2

Figure 4.9 Buckled, Longitudinal No. 8 Reinforcing Bar in the Top Bell of the Girder

Figure 4.10 West Elevation of Damage Received During Test C2

4.3 Results & Conclusions

4.3.1 Material Testing Results

Upon completion of testing, a total of six cores were extracted from the web of the girder in addition to three cores from the deck for evaluating compressive strength and modulus of elasticity. Two samples of prestressing strand were also tested from a similar girder (girder "A" in Murray's study) for tensile strength as well as modulus of elasticity. Compressive testing results from the web and deck core samples bore average strengths of 7,180 psi and 6,060 psi, respectively. The samples of prestressing strand were confirmed to be Grade 270 with average tensile strengths of 283 ksi and an average modulus of elasticity of 26,350 ksi. Furthermore, samples of shear reinforcing used in the beam were tested to determine the yield stress, ultimate strength, and modulus of elasticity. The average resulting values illustrated that the steel matched the drawings issued by ODOT in that the steel was, in fact, Grade 40.

4.3.2 Load-Deflection Test Results

Figure 4.11 and Figure 4.12 illustrate the load versus deflection plots for the C1 (south end) and C2 (north end) Tests, respectively. Complications during test C1 and C2 led to multiple loadings for each test. Each of the loadings for test C1 and test C2 are plotted with the exception of the first loading for test C1. That test, C1a, was stopped before cracking and the girder maintained its linear-elastic behavior. At an applied load of nearly 230 kips, the wire potentiometers began to record inaccurate deflections for test C2 and, thus, manual measurements had to be logged. These supplemental measurements have been accounted for in the plot. The results of tests C1 and C2 are detailed in Table 4.1. Ultimately, the failure mechanism that was pinpointed for the C1 Test was bond-shear failure and the C2 Test was found to be a compression-shear failure. It was believed that the visible corrosion at the ends may have contributed to the debonding of the strands in test C1 at the south end. Murray continues with a comparison of the calculated capacities compared to the several design methods stated previously. These comparisons are excluded here but are discussed thoroughly in Murray's dissertation (Murray, 2017). Elevation drawings mapping the scope of damage from testing can be found in Appendix A.

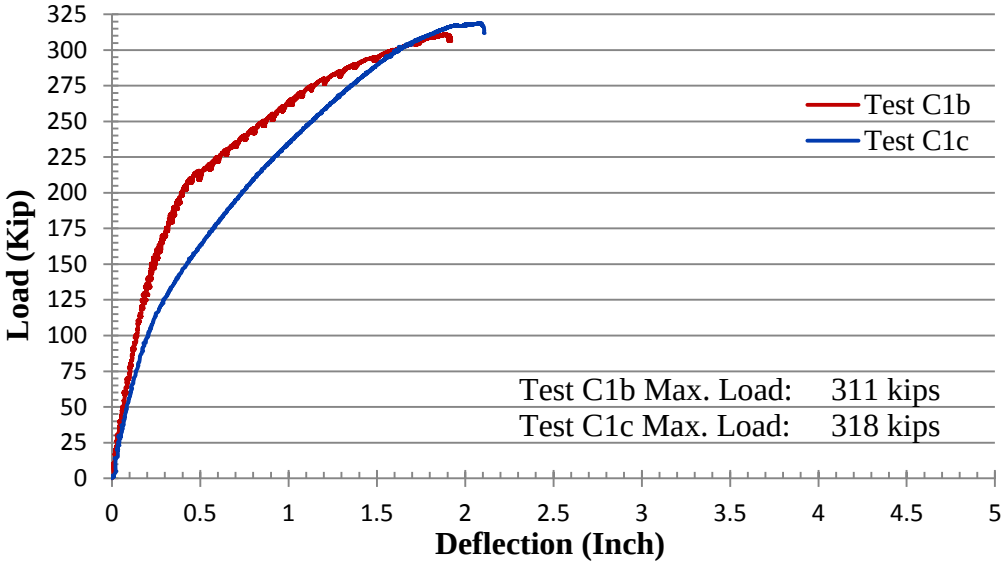

Figure 4.11 Load vs. Deflection Plot for Test C1

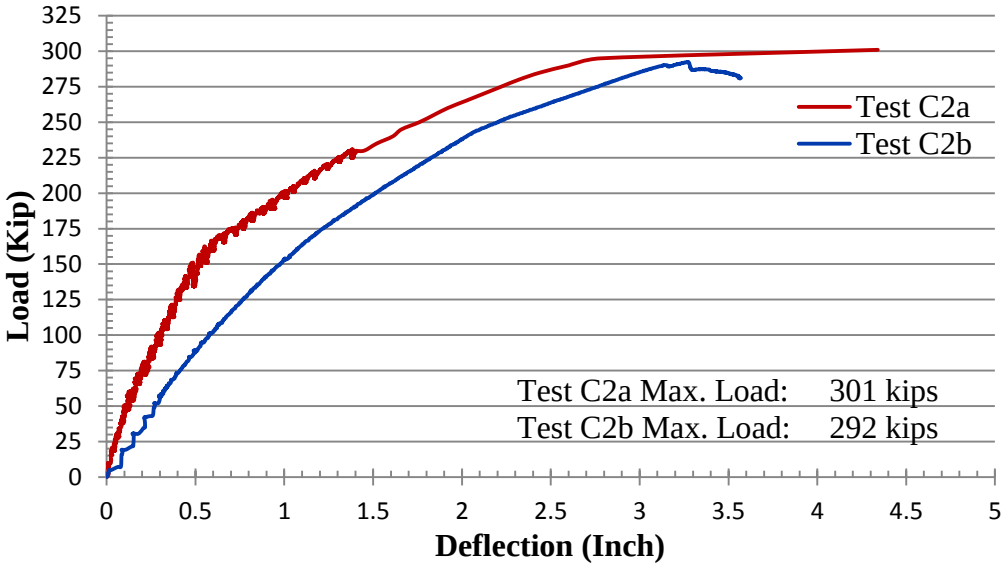

Figure 4.12 Load vs. Deflection Plot for Test C2

Table 4.1 Testing Results for Girder C

Properties	C1	C2
Span	25 ft.	28 ft.
Cracking Load	160 kips	150 kips
Observed Cracking Moment	904 kip-ft.	1030 kip-ft.
Max Load	318 kips	301 kips
Max Shear	204 kips	179 kips
Max Moment	1832 kip-ft.	2040 kip-ft.

Chapter 5: Repair of AASHTO Girder

Upon conclusion of the studies performed by Murray on the girder described in the previous chapter, the research and application of the repair process began. The process and development of the repair for each section is discussed in this chapter. There are three main areas of repair for the girder: the core-sampled web section just south of the diaphragm at midspan, the south end, and the north end.

5.1 Core-Sampled Web Repair

5.1.1 Extent of Damage & Concrete Removal

Before any of the large repair sections were recast, a pilot repair section was conducted on an area of the girder that was used to retrieve core samples for the previous testing. Previous researchers, in an attempt to attain acceptable core samples, inadvertently cored through the shear stirrups in the web of the girder. Upon retrieving acceptable core samples, the web section was left with seven holes about 4” in diameter and a single half-drilled hole of the same diameter. A rectangular zone of 4 feet, 5 inches in length (in the direction of the span) by 1 foot in height was marked out. This size was used in order to encapsulate all the borings into a single repair (see Figure 5.1 for pre-repaired elevation). Concrete within that zone was removed using a grinder and hammer-drill. It was found that because of the arbitrary location of the corings and their proximity to the upper and lower bounds of the web, the initially allocated zone needed to be expanded

to allow for proper splice lengths for the reinforcing steel that was severed. Some of the corings did not fully sever some of the reinforcing bars. The damaged area of these bars were removed by grinding just above and below the damaged area. The final removal area measured 4 feet, 7 inches in length and the total height of the web section, 1 foot, 3 inches, with seven damaged stirrup legs.

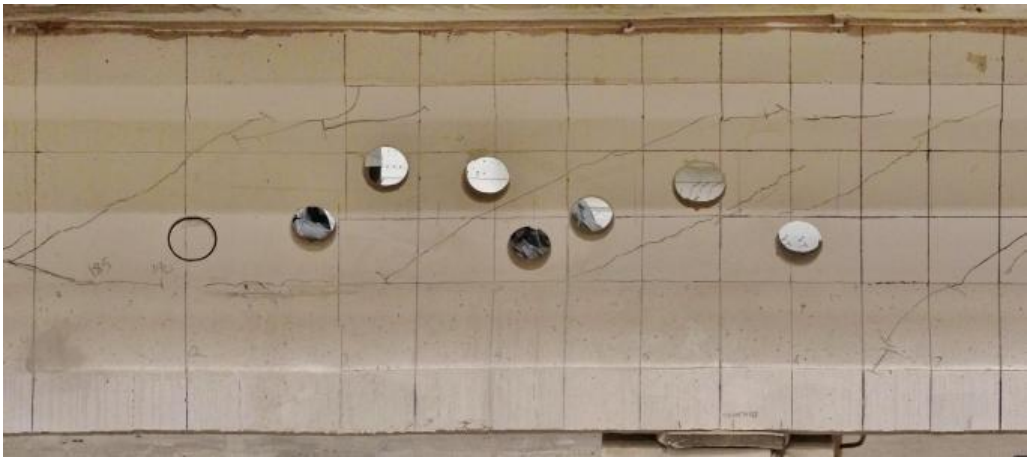

Figure 5.1 West Elevation of Core-Sampled Web Section

5.1.2 Formwork Design & Construction

Formwork for the repair was predesigned using a three-dimensional modeling software called SketchUp. Once a formwork design was accepted, it was constructed using 3/4-inch plywood and standard 2x4 (nominal) lumber that was cut to specified lengths. Supporting 2x4s lined the edges of the plywood and vertical rib supports were spaced at 12 inches on center. All lumber was fastened to the formwork using 3-inch wood screws spaced at 12 inches on center. The east side form had two 1 inch deep holes cut in the top edge of the form so that air

could escape and the concrete level could be monitored during the pour. The plywood surface exposed to the repair concrete was coated with polyurethane to help preserve the formwork. After the polyurethane dried for 24 hours, they were braced against the repair area to determine placement for the threaded rods that would fasten the forms together. The threaded rods were 18 inches long, 1/4-inch diameter stainless steel with matching nuts and washers. Wooden blocks were cut and drilled to act as an additional washer and to keep the formwork from deforming around the rods. To place the new concrete into the formwork, 4 inch diameter PVC was selected as the fill neck for the formwork (Figure 5.2). This PVC size was chosen based on the mix design study discussed in Chapter 3. A single section of pipe with an angle joint at each end was used as the fill neck. A wooden base was constructed around the lower end of the fill neck so that it could be fastened to the formwork using screws. A bead of silicone was added to the edges of the formwork and top end of the PVC fill neck to maximize containment of the concrete.

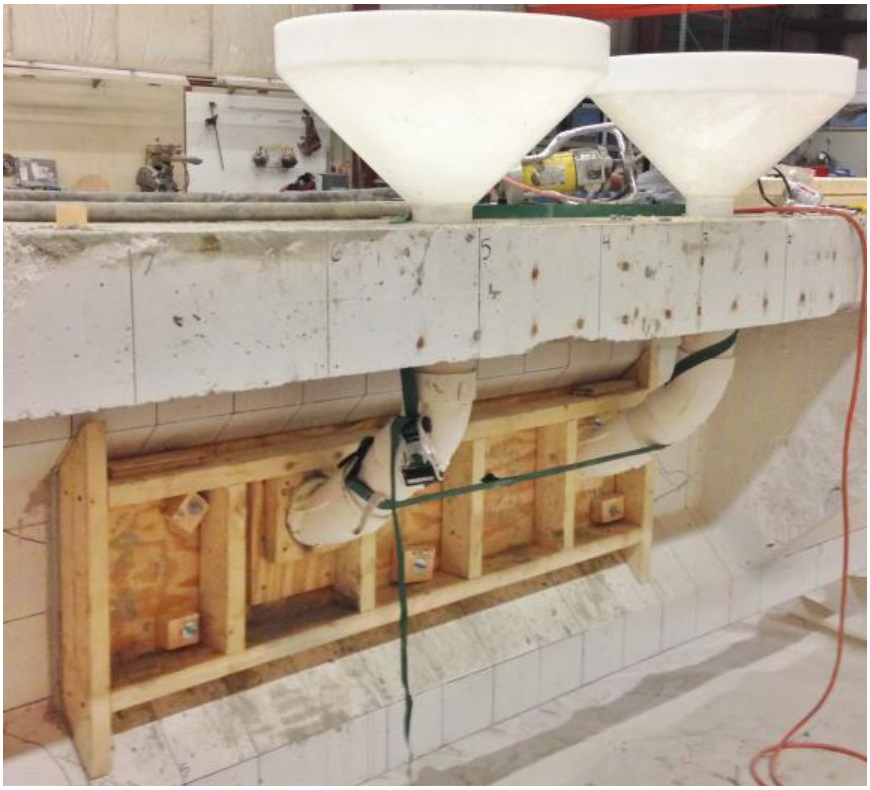

Figure 5.2 Assembled Formwork, Core-Sampled Web Repair

5.1.3 Repair of Internal Reinforcing

The existing shear stirrups were constructed using Gr. 40, No. 4, deformed steel bars and the splicing steel was of the same type and grade. The splicing bars were connected to the existing reinforcing using BARSPLICE™ couplers specifically sized for the reinforcing bars being used. Figure 5.3 shows the installed couplers for the repair. Additionally, the couplers are designed to meet the ASTM requirements for bar splicing. Before these couplers were fully secured, they were test fit to allow for the maximum distance between splicing materials and the surface of the formwork. The couplers' tightening mechanism featured snap-off bolts that sheared off once the bolts were tightened to the

manufacturer's specified torque of 720 inch-lbs. To ensure consistency, the bolts were tightened using a torque wrench set to match the specified capacity previously mentioned.

Figure 5.3 Core-Sampled Web Replacement Reinforcing

5.1.4 Placing the Repair Concrete

The initial pour of the pilot repair section was performed during the first week of August of 2016. The ambient temperature during this time ranged from the upper 90° F up to and occasionally beyond 100° F. It was decided that, since this temperature range falls outside of the ASTM recommended temperature range for mixing and placing concrete, the mix materials had to be chilled overnight before mixing. The materials were batched into 5-gallon buckets with rubber-sealed lids. The buckets that held aggregates were placed into large water troughs, covered with transparent trash bags, then ice was added to the troughs as shown in Figure 5.4. The troughs, along with the remaining materials, were housed in an environmental chamber that maintains a consistent temperature of 70° F.

Figure 5.4 Mix Materials Chilled with Ice

On mix day, a mixture of ice and water was placed in the mixer and agitated for 20 minutes to cool the mixing drum and saturate the surface of the mixer. The ice water mixture was drained while the lever-operated, concrete dispensing bucket was rinsed out with a water hose. The materials were then removed from the environmental chamber and added into the mixer in accordance with ASTM C192/C192M-16a (2016). Upon adding the fine aggregates, it was discovered that some of the ice had melted in the troughs and the water had leaked into some of the buckets. To counter the unanticipated water, the sample was weighed and the weight difference between the original weight of the aggregate and the weight with the water was recorded. That difference was used to reduce the appropriate amount of water to be added later.

During the final stages of mixing, when adding the admixtures, the concrete started to experience signs of premature setting along with segregation of

the aggregate and cementitious paste. This became more evident when transferring the mix to the dispensing bucket and when adding it to the formwork. The quicker set time and segregation caused the aggregates and the fibers to collect at the bottom of the bucket and clogged the fill neck despite trying to consolidate the mix using a tamping rod. It was decided to abandon this mix and try again. As a result, the remaining concrete was disposed of and the formwork removed and cleaned. Figure 5.5 shows how much the form was able to be filled. Any concrete material in the form and fill neck was removed and the surface was cleaned with a wet towel and compressed air. It is believed that multiple factors played into the failure of the mix: extreme temperatures, unanticipated leaking of ice water into the aggregate buckets, abnormal absorption by the aggregates in those buckets, but the most likely cause was the use of a different high-range water reducer than used in previous mixes.

Figure 5.5 Extent of Flow for First Pour of Core-Sampled Web

The second pour for the pilot repair section used the same proportions of materials as the previous pour (see Chapter 3, Table 3.3) with one exception: a

higher dosage of citric acid was used (the adjusted proportions are given in the following section). Moreover, at the time of the second pour, the ambient air temperature was much cooler and no extra measures needed to be taken to maintain an ASTM approved mixing temperature. The mixing was performed in accordance with ASTM C192/C192M-16a and added to the formwork until the concrete filled the forms. It was observed that this pour also had a faster set time than anticipated. However, the forms were filled, leaving only a small 1/8 inch gap or less on the tops of each side of the web (see Figure 5.6). This could be due to the quick set time of the concrete and/or because the fill neck was connected toward the mid-height of the forms, forcing the mixture to have to fill the form from the midsection upwards.

The formwork was removed after the concrete was allowed to cure for 24 hours. Since there was concrete trapped inside the fill neck, a grinder was used to cut away the fill neck piece by piece until the side forms could be removed. The stainless steel threaded rods that were used to hold the formwork to the beam were cut at the face of the concrete and the section of concrete where the fill neck connected to the forms was ground flat to match the surface of the web section. Several months later mortar was added to the gap at the top of the repair section between the bottom of the existing beam and the top of the new, repair concrete. The mortar mixture was based on the traditional 3-2-1 mix design: 3 parts fine aggregate, 2 parts cement, and 1 part water. The mortar mix was placed into the gaps using putty knives and allowed to cure several days before grinding the

excess mortar flat, matching the surface of the beam. No additional test specimens were made at the time of casting.

Figure 5.6 Core-Sampled Finished Repair (Without Mortar Patch)

5.2 Repair Mix Design Modifications

After the Core-Sampled Web Repair, Dolese, a local materials provider, ceased to carry MasterGlenium 7500 produced by BASF, the Type A/Type F high-range water reducing admixture that was used in the original research and development of the fiber-reinforced, self-consolidating concrete (FR-SCC). This forced the research team to select a new admixture based on Dolese's availability. The new high-range water reducer (HRWR), MasterGlenium 7920 also by BASF, is a verified Type A/Type F admixture in accordance to ASTM C 494. The original mix design that utilized the MasterGlenium 7500 called for 9.0 fl. oz/cwt, which was the nearest, whole unit of measure to the median for the manufacturers

recommendation for dosage of the admixture (2 to 15 fl. oz/cwt). Similarly, the proportions of the MasterGlenium 7920 were originally selected based on the recommended dosage by the manufacturer of 2 to 12 fl. oz/cwt. Using the original target slump flow of 28 inches, the proportions of the new HRWR were refined by conducting trial mixes. The resulting dosage of MasterGlenium 7920 that yielded a 28-inch slump flow was 8.25 fl. oz/cwt. Final mix design proportions are listed in Table 5.1 and Table 5.2.

Table 5.1 FR-SCC Mix Design Specifications

Cementitious Amount, lb./yd^3	750
Class C Fly Ash Replacement (by mass), %	30
Komponent Replacement (by mass), %	15
w/c Ratio	0.38
Amount of Fine Aggregate (by volume), %	50
MasterFiber MAC Matrix (by volume), %	0.5
Target Slump Flow, in.	28.0

Table 5.2 FR-SCC Mix Design Proportions, Saturated, Surface-Dry

Type II Cement, lb./yd^3	412.5
Class C Fly Ash, lb./yd^3	225.0
Komponent, lb./yd^3	112.5
Water, lb./yd^3	281.5
Fine Aggregate, lb./yd^3	1403.6
Coarse Aggregate, lb./yd^3	1261.3
MasterFiber MAC Matrix, lb./yd^3	7.7
Air Entrainment Master Builders AE-90, oz/cwt	1.1
Water Reducer Glenium 7920, oz/cwt	8.25

5.3 South End Repair

5.3.1 Extent of Damage & Concrete Removal

Once surveying and documenting of the initial, failed state of the girder was completed, shown in Figure 5.7, preparation started for the south end to be repaired. Using the survey data, an extent of concrete was designated for demolition and repair. The original extent measured 8 feet from the southern face of the girder and one foot perpendicular from the bottom face of the girder. The aim in doing so was to maintain an area defined by 6 inch increments of the preexisting grid mapped on the girder in previous testing and to reduce the number of irregular shapes in the repair section. This area to be demolished encapsulated the entire bottom bell of the girder for the 8-foot section.

However, due to the presence of large cracks at the intersection of the eight foot marker from the end of the girder and one foot boundary from the base of the girder, the area was expanded to include these cracks in the repair section. Expanded boundaries of the repair were moved to 8 feet, 2 inches from the southern face of the girder and the top boundary was raised from one foot to 1 foot, 3 inches only from the 6 foot mark from the southern face until the 8 foot, 2 inch boundary. The southern face of the girder features an 8-inch-thick diaphragm that was cast onto the member during its original installation within the bridge structure. When the 10-inch-thick deck addition was fabricated in Murray's study, the addition did not extend fully to the end of the girder. Rather, the addition was cast up to 8 inches shy of the end of the girder. The missing 8 inches of deck on

the west side was utilized as the planned fill hole for the FR-SCC repair material. Since the diaphragm was cast onto the girder post-installation with no roughening of the interface between the girder and diaphragm, removal of the west side of the diaphragm was achieved with relative ease in comparison to the concrete on the girder itself. In order to provide for a better bond to the surface of the girder and west-side deck extension, the surfaces were roughened using a hammer-drill. An illustration of the final, fully demolished South end is shown in Figure 5.8.

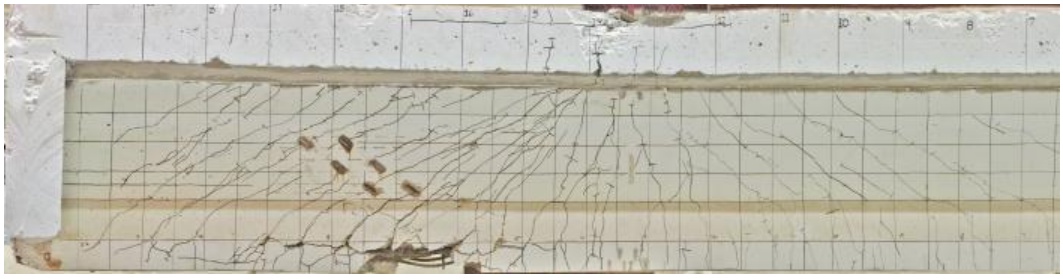

Figure 5.7 South End Damage From Original Testing

Figure 5.8 South End With Damaged Concrete Removed

5.3.2 Formwork Design & Construction

Subsequent to the demolition of the south end, formwork for the corresponding area was designed and constructed. The design was conceived using SketchUp in conjunction with the actual measurements from the girder and known, available lumber sizes. In the best interest for section continuity, the decision was made to try to retain the original shape and aesthetics of the girder for the repair volume with minimal exceptions. The only exception was that the south end diaphragm would be the full height of the girder as opposed to the original diaphragm size that extended down from the deck to the top of the bottom bell section of the girder with a 45-degree angle extending from the mid-height of the bell up to the diaphragm section. Figure 5.9 shows the formwork rendering that was created using SketchUp. The total volume of replacing concrete to fill the formwork was 15.20 cubic feet, not accounting for the volume of reinforcing material in the section.

To properly brace this amount of material, standard 2x4 sawn lumber and 3/4-inch-thick plywood were the base materials to construct the formwork. Each panel of the formwork was constructed with 2x4's fastened to the perimeter of the plywood using screws. All formwork pieces for the girder featured vertical, intermediate bracing at 12 inches on center. Vertical, intermediate bracing varied depending on the shape and protrusions of the diaphragm forms. Upon completion of the formwork construction, the faces of the individual sections were coated with a single, thick coat of polyurethane and a form release agent. The

polyurethane coat acted as a protective layer to preserve the formwork for reuse later in the project while also allowing for a smoother concrete surface. The form releasing agent reacts with the alkalinity of the concrete during casting to create a film-like layer of foam, preventing any bond between the concrete and forms.

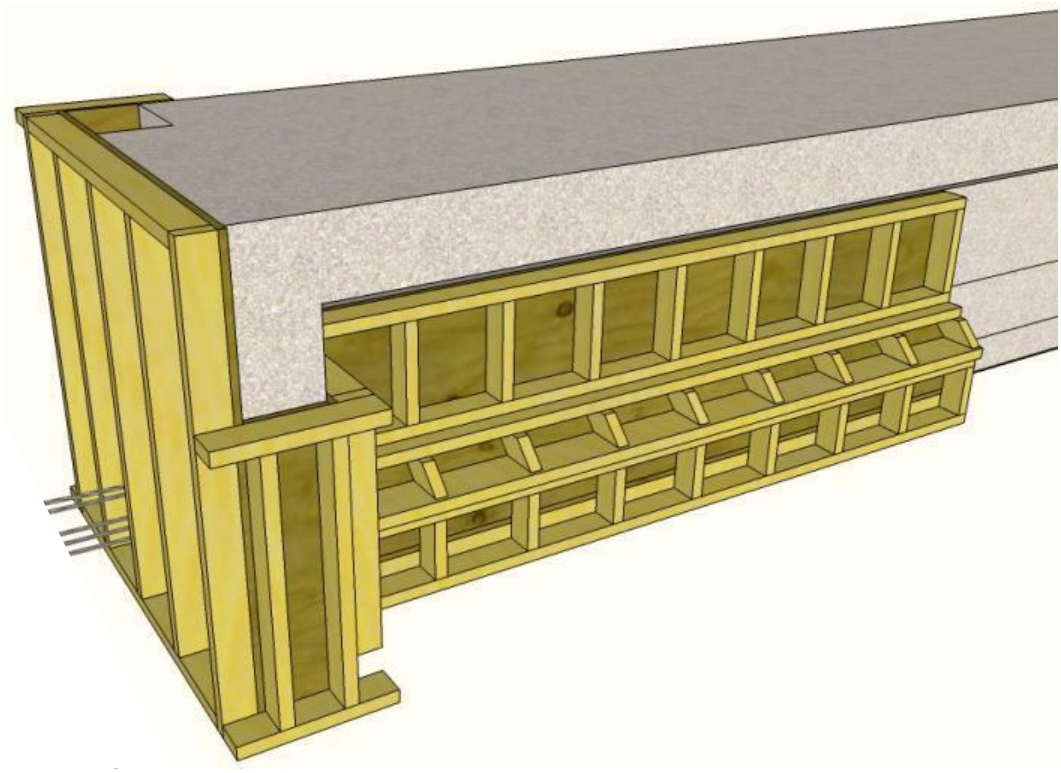

Figure 5.9 South End Formwork SketchUp Design

5.3.3 Repair of Reinforcing

As part of the repair solution, the prestressing strands originally housed in the bottom bell needed to be re-tensioned. Achieving the reapplication of this prestressing force was performed by post-tensioning the existing tendons. However, the tendons in the girder were terminated at the ends of the girder, making it impossible to have sufficient length of material to post-tension with the

existing strands. Furthermore, the ends of the strands showed signs of corrosion to the extent that they would have been inadequate for restressing. As a result, the existing strands were cut to a shorter length, within the repair section, and new strands were connected using Sure-Lock® 1/2 inch splice chucks. Due to limited availability, the replacing tendons are 1/2 inch special as opposed to the existing, 1/2 inch tendons in the girder. Splice locations depended on the layout and fitment of the splice chucks with their housings; by staggering the splice chucks, all ten strands were able to be spliced within the bottom bell of the repair volume, which is shown in Figure 5.10. Existing tendons were cut at a dimension that allowed for them to protrude 1/2 inch beyond the wedges within the splice chuck (Figure 5.11). The remaining lengths of exposed existing and replacement strands were coated in a thin layer of automotive grease, then sleeved with a 1/2 inch plastic irrigation line. This grease-and-sleeve arrangement, shown in Figure 5.12, is similar to monostrand post-tensioning tendons and allows for movement during the post-tensioning stage.

A special housing was created using a clear, acrylic sheet and foam cutouts to permit movement of the splice chucks during tensioning. Construction of the housings began with forming the acrylic sheets to a cylindrical shape by heating them in a uniform manner, minimizing warping. A 2-inch-diameter PVC pipe was used as the template for molding the curvature of the sheets. Once cooled, a splice chuck was placed in the now cylindrical, acrylic sheet, and the sheet was clasped tight around the chuck and secured by wrapping it with clear

packing tape. The result was a transparent tube for the splice chuck to slide through. Each end of the tube was filled with foam to prevent concrete from entering the tube. The foam used for the ends was a heavy grade floral foam and was chosen for its resilience under moderate pressure but would still compress under higher pressure.

Figure 5.10 Assembled Post-Tensioning Splice Chucks

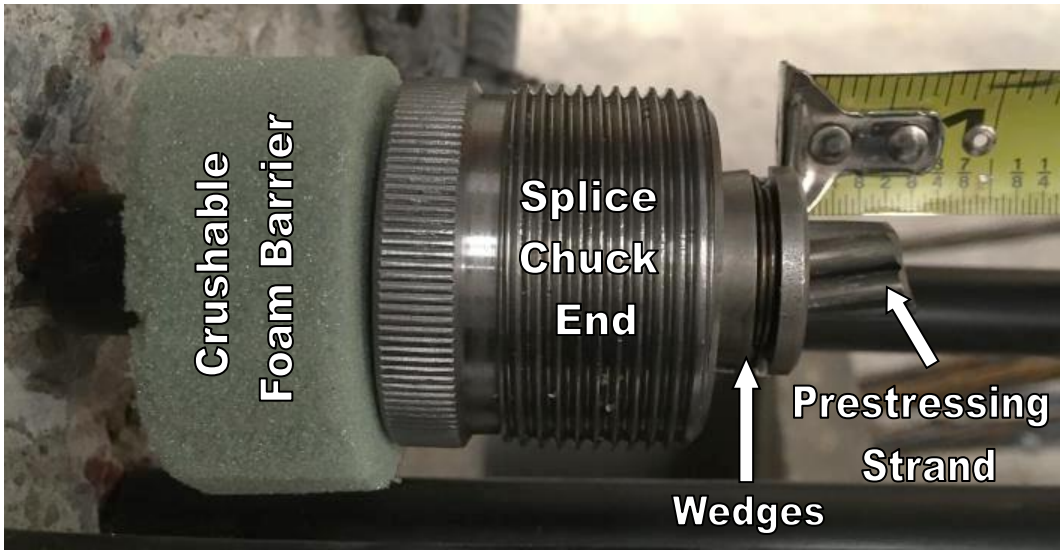

Figure 5.11 Splice Chuck Assembly for Existing Strand

Figure 5.12 Post-Tensioning, Grease-and-Sleeve Arrangement

The aforementioned assembly of strand components for post-tensioning was a methodological procedure. To start, the greased-and-sleeved segments were marked for the existing and replacing strands. These segments extended from the face of the existing concrete to the face of the splice chuck, then from the opposite

face of the splice chuck to the inside face of the post-tensioning anchors. Following the greasing and sleeve placement on the existing strand, one of the foam pieces were slid over the sleeve and one end of the splice chuck was attached and seated to the end of the existing tendons. The shaft of the splice chuck was then assembled to the end of the splice chuck that was attached to the existing tendon and the replacing strand with the other end of the splice chuck was subsequently attached to the splice chuck shaft. Tongue-and-groove pliers were required for tightening the two ends of the splice chuck due to the internal, spring-loaded mechanics of the splice chucks, but, consequently, ensured proper seating of the wedges on both strands before tensioning. Grease was applied to the replacing strand and sleeved before the acrylic tube and other foam piece was slid over the sleeve and splice chuck, completing the housing assembly. Figure 5.13 shows the full post-tensioning assembly.

Figure 5.13 Fully Installed Post-Tensioning with Partial Formwork

The final preparation before assembling the formwork and pouring the repair section was to add bursting steel. Bursting steel is used to resist the Poisson's effect that can lead to failure during the post-tensioning of a section. As opposed to pretension applications were the stress from the tendons is transferred to the concrete throughout the length of the member, post-tension applications collectively apply the full force of the tendons at the anchored ends. High concentrations of compressive stresses in a single direction causes expansion in the perpendicular directions, which has the ability to be somewhat explosive for concrete applications. Thus, the use of additional, confining reinforcement just inside of the anchored regions is essential. Using various iterations of strut-and-tie modeling, a conservative calculation for the appropriate amount of steel was selected. Four pairs of closed loop, No. 3 bars with two inches of clear spacing were added to the section for a total of eight bars. To maximize the area of confinement, the bars were bent in the same shape as the bottom bell while permitting for one inch of cover on all sides. Addition of the bursting steel, shown in Figure 5.14, marked the completion for reinforcing the interior of the south end. The final preparation step for the prestressing tendons involved installation of monostrand anchorages for each strand, which were threaded over the strands and nailed to the inside face of the form end.

Figure 5.14 Bursting Steel for Post-Tensioning

5.3.4 FR-SCC Monitoring Formwork Additions

The final measure of preparation for casting was to assemble the forms and seal them for the FR-SCC. As mentioned previously, the fill location is located at the south diaphragm and the FR-SCC would then be allowed to flow through the diaphragm, down the length of the repair section and up 3 inches into the web section. Figure 5.15 illustrates the general passage for the FR-SCC. To accommodate this rise, a single, 2-inch-diameter vent hole was created on one side of the web form. The vent was located at the midpoint of the top edge of the raised section. On the opposing side a small window was added to monitor the FR-SCC height during casting. The window was also 2 inches in diameter and made from a sheet of acrylic. Two 12-inch-long LED light strips were

countersunk into the interior face of the web form featuring the window, providing for enhanced viewing inside the forms. Included with the packaging of the light strip was a toggle button to activate the lights, this was mounted to the exterior side of the form for use while looking through the window (Figure 5.16).

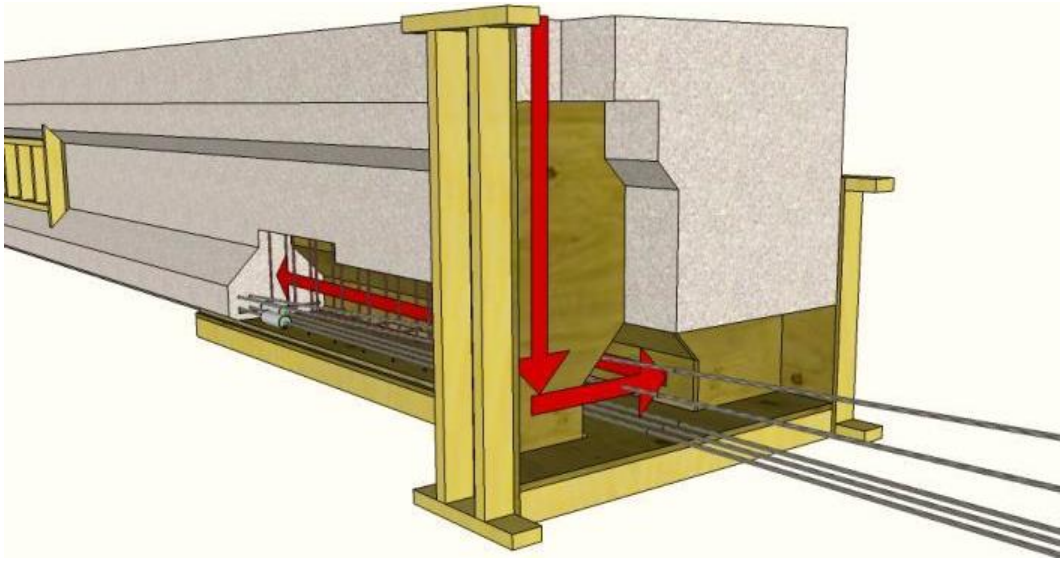

Figure 5.15 South End Repair Concrete Flow

Figure 5.16 Observation Window for Monitoring Flow (Left) and View Through the Window (Right)

5.3.5 Placing the Repair Concrete

A total amount of concrete chosen for casting was 16 cubic feet. This amount would be able to fill the repair volume with almost an extra cubic foot of contingency. The capacity of the available onsite mixer is 17 cubic feet of normal concrete and, therefore, it was concluded that the small-scale specimens would be cast at a later date. The ensuing days before casting, all the materials were batched into large crane-hoisted, buckets and 5-gallon buckets. The coarse and fine aggregates were collected in the larger buckets, both were covered with a plastic tarp over the top and sealed with tape. As the materials were batched, small samples of each were obtained for a representative moisture content testing of each aggregate. All cementitious materials, fibers, and water were placed into 5-gallon buckets with sealed lids. Citric acid, the set-retarding admixture, was batched into multiple small plastic containers with a single dosage per container.

On casting day, but before mixing, the air entraining admixture was poured into the fine aggregate and the HRWR was gathered into large graduated cylinders. As the mixer was turning, the aggregates were added, first course, then fine aggregate was added. Half of the water was poured into the mixer followed by all the cementitious material. The consistency of the mix at this point is very thick and tends to turn in the mixer as a solid mass. The rest of the water is immediately added to the mix, allowing the mix to appear like a stiff, low slump concrete. It should be noted that in the research performed by Wirkman, the concrete was mixed for 4 minutes preceding the addition of the high-range water-reducer, however, it was found in early trials of this study that this step was unnecessary and excluded in the interest of preserving time for this study.

The high-range water-reducer was added at approximately 50 mL per second and was distributed evenly in the mixer. The remaining citric acid, diluted in water, was added followed by the fibers. After the fibers were sprinkled into the mixer, the materials were allowed to mix for 3 minutes, rest for 3 minutes, then mix again for a final 2 minutes following conditions set by ASTM C192/C192M – 16a. An additional dosage of citric acid was added at the end of this period and permitted to mix for 1 minute before the concrete was dispensed into a crane-hoisted bucket for transport to the repair section. Monitoring the FR-SCC through the fill location and the window in the web, the mix was able to flow around the internal reinforcing filling the entire form. After the form was filled, a slump flow test was performed and 3 cylinders were cast with the excess

concrete. The slump flow results yielded a 26.5 inch slump flow and the cylinders were set aside for compression testing when the repaired girder was tested. Upon completion of casting, the top of the form and the small specimens were covered with a plastic sheet for seven days, then the forms were removed. Figure 5.17 shows the seven-day-old repair section following form removal.

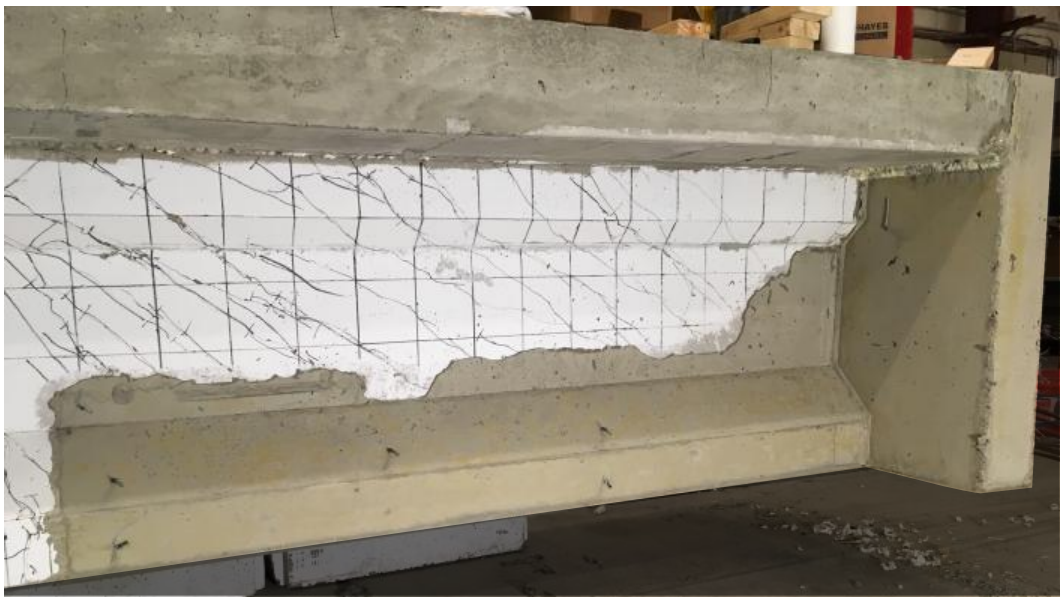

Figure 5.17 South End Repair with Forms Removed

5.3.6 Post-Tensioning the Repaired Section

Upon removal of the formwork of the south end, it was observed that some of the FR-SCC repair material had seeped into the holes of the anchor plates through which the strand passes (Figure 5.18). This volume is the conical region where the wedges would set for post-tensioning; thus, it was important for this location to be cleared of obstructions, allowing for proper seating of the wedges.

To remove the excess concrete, a hammer and various small chisels and picks were used to break away some of the existing concrete. In an effort to expedite the clearing of the anchor plates, an alternative approach was conceived that included prying the anchor plates away from the concrete to better remove the excess concrete. In doing so, concrete was spalled off the bearing area for the only two anchor plates removed, shown in Figure 5.19. It was decided to cease progress with this approach and instead utilize a high-velocity pressure washer to clean-out the remaining concrete in the anchor plates.

Once the excess concrete was removed, a mixture of mortar was used to patch the spalled concrete behind the two anchor plates removed previously. This mixture included sand, Type III portland cement, hydrated lime, and water. The material mix ratio was three parts sand, one part cement, one-fifth part hydrated lime, and one-third part water. The mixing method closely followed the ASTM recommended procedure for test specimens in the lab (ASTM C192). All materials excluding water were mixed together, thoroughly. Water was added to the mixture and hand mixed for 3 minutes. The mixture was allowed to rest for 3 minutes while water was brushed on the application area of the girder, then mixed again for 2 minutes. The mortar was applied by hand initially and spread with a putty knife. Immediately, the anchor plates were pressed against the girder and tapped with a rubber mallet to provide for consolidation of the mortar. The plates were clamped in-place and allowed to cure for 7 days until post-tensioning was performed on the section.

Figure 5.18 Anchor Plates After Casting the South End Repair

Figure 5.19 Damaged Area After Removal of Anchor Plate

Post-tensioning was performed by stressing individual strands up to the originally specified 28.8 kip load per the ODOT construction documents. In doing so, the inner most strands were stressed first, alternating from each strand group on each side until the outermost strands were the last to be tensioned. Figure 5.20 illustrates the pattern in which the strands were tensioned, and Figure 5.21 shows the tensioning setup. Stressing was achieved by using a monostrand post-tensioning jack manufactured by Precision-Hayes International that was attached to a motorized, hydraulic pump featuring a pressure gauge. A load calibration test was conducted with the same equipment before post-tensioning to determine the gauge reading that coincides with a 28.8 kip force in the strands. Since the monostrand jack includes a power-seating device, very minimal seating losses occurred and all strands were successfully re-tensioned. The strand tensioner achieves re-tensioning by pushing against the anchor plate and pulling the strand. Once fully tensioned, a second internal cylinder seats the wedges in place, approximately maintaining the desired strand force of 28.8 kips.

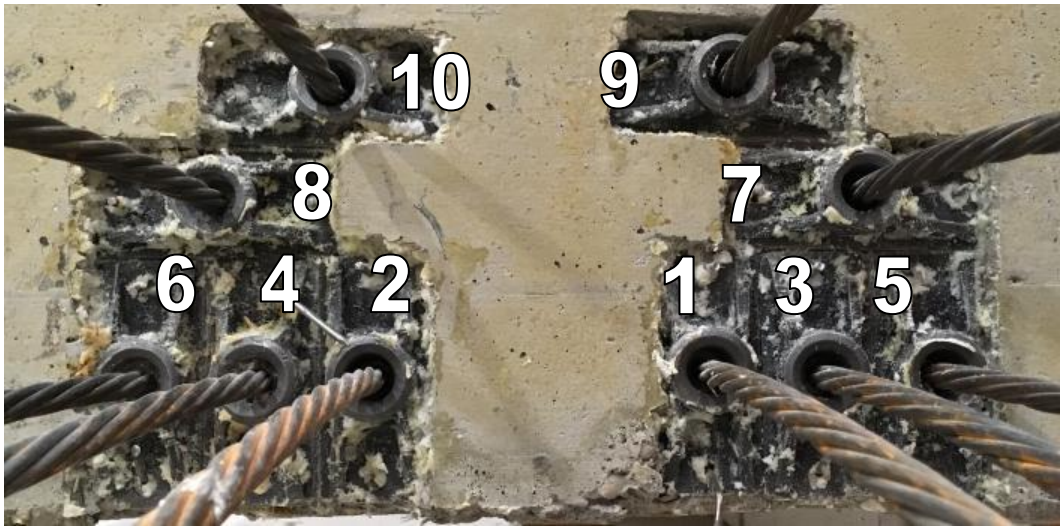

Figure 5.20 Post-Tensioning Stressing Order

Figure 5.21 Post-Tensioning Strand Stressing

5.4 North End Repair

5.4.1 Extent of Damage & Concrete Removal

In the best interest of safety, major demolition of concrete did not start until the south end was cast and the strands re-tensioned. Upon initial surveying of the north end (Figure 5.22), the beam did not appear to have significant damage and that the repair would have been limited to the deck and bottom bell where horizontal cracks showed signs of possible debonding. However, during the demolition, it was discovered that beyond the surface, the north end had major damage to the concrete that extended from the top of the deck to the bottom bell. The concrete in this zone was loose enough that portions of it fell off without agitation. This damage, as illustrated in Figure 5.23, followed a 45-degree angle extending from the load point diagonally down to the north support (the closest support to the load point). As a result, the demolition area was expanded to where the southern boundary for the girder was along the 11 foot gridline (measured from the midpoint of the girder) and the southernmost boundary for the deck was four inches north of the 10 foot gridline. The northern boundary for the deck was along the 16 foot gridline as well as the top bell portion of the girder. The northern boundary for the web of the girder coincided with the 16.5 foot gridline and the bottom bell boundary was 18 inches to the north of that at the 18 foot gridline. Figure 5.24 shows the full extent of the concrete demolition.

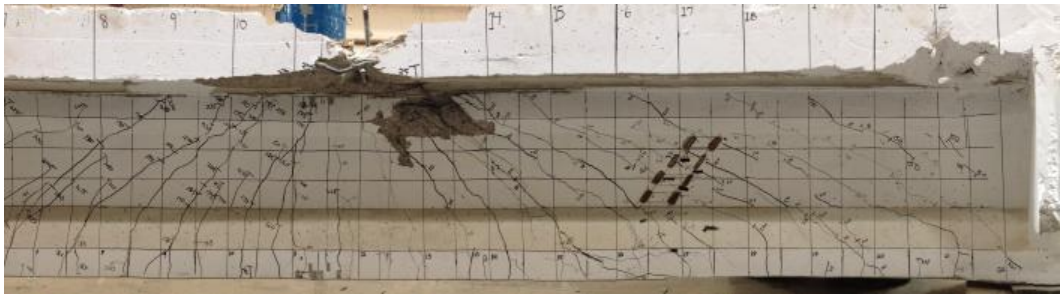

Figure 5.22 North End Damage from Original Testing

Figure 5.23 Further Damaged Concrete Uncovered During Demolition

Figure 5.24 North End with Damaged Concrete Removed and Loose, Existing Reinforcing Steel

5.4.2 Formwork Design & Construction

The formwork that was used for the south end repair was able to be reused for the north end due to the special care for constructability that was taken into account during its design. New formwork was only needed for the top bell of the girder and the deck. Using the same techniques for construction as previously discussed, the top bell and deck forms were built so that the girder would be cast first, then the deck cast at a later date. The window that was included in the south end repair happened to be covered by existing concrete on the girder, so it was not used for this placement. Additionally, since this placement did not require the concrete to travel down through the formwork and back up like the south end repair, it was deemed unnecessary to have a window in the formwork, nor was it necessary to have vent holes. An illustration of the forms for the north end via SketchUp is shown in Figure 5.25.

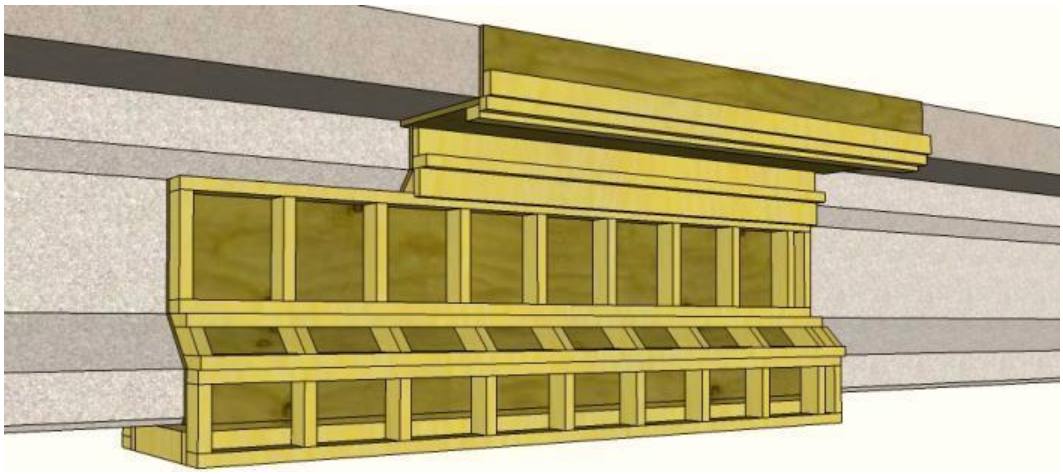

Figure 5.25 North End Formwork SketchUp Design (West Side)

5.4.3 Repair of Girder Reinforcing

Originally, the girder was cast with two grade 40, Z-bar stirrups at spacing that is specified in the original ODOT drawings. A typical arrangement for the internal reinforcing is shown in Figure 5.26. As the area of repair features the entire height of the girder and deck for at least 5 feet, almost all the existing reinforcing was either replaced or altered in some way. The original reinforcement for the girder for this section included two Z-bar stirrups at 8 inches on center, since the repair area falls within the *0.3*L*, or 14 feet, from the end of the girder. The height of the draped strands are approximately 1 foot, 8 and 3/8 inches on the high side (north boundary of the repair) and 1 foot, 1 and 7/8 inches on the low side (south boundary of the repair) measured from the base of the bottom bell to the center of the two lowest, draped strands. Within the area of

the top bell there are two longitudinal No. 8 reinforcing bars that buckled away from the center of the cross section in the original testing.

The deck reinforcing was a collection of longitudinal and transverse reinforcing bars that were not symmetric to the vertical axis of the girder. All the longitudinal deck reinforcing bars were No. 4 bars, while the transverse bars were No.5 bars. The east side of the deck contained two longitudinal bars placed at about a quarter of the deck width and one above the other. The west side also only had two longitudinal No. 4 bars about 2 inches from the west face of the original deck. However, with the deck extension that was added before the original testing, four additional reinforcing bars were included in the west side of the deck, one in each corner of the extension cross section.

Figure 5.27 shows the north boundary of the repair with the longitudinal bars of the deck and girder. The transverse bars, according to ODOT's drawings, were alternating bar shapes that were No.5 bars spaced at 10 inches on center (5 inches on center between bar types). The two bar types were one grouping of two straight No. 5 reinforcing bars, one at the bottom of the deck and the other placed at the top of the deck in line with the bottom bar. The second bar type was a bent No. 5 bar where the shape allowed for the bar to be a top bar over the girder and a bottom bar in the span between girders. A diagram for the layout of a typical section of the deck is shown in Figure 5.28, and Figure 5.29 illustrates a partially demolished deck portion with the original transverse reinforcement.

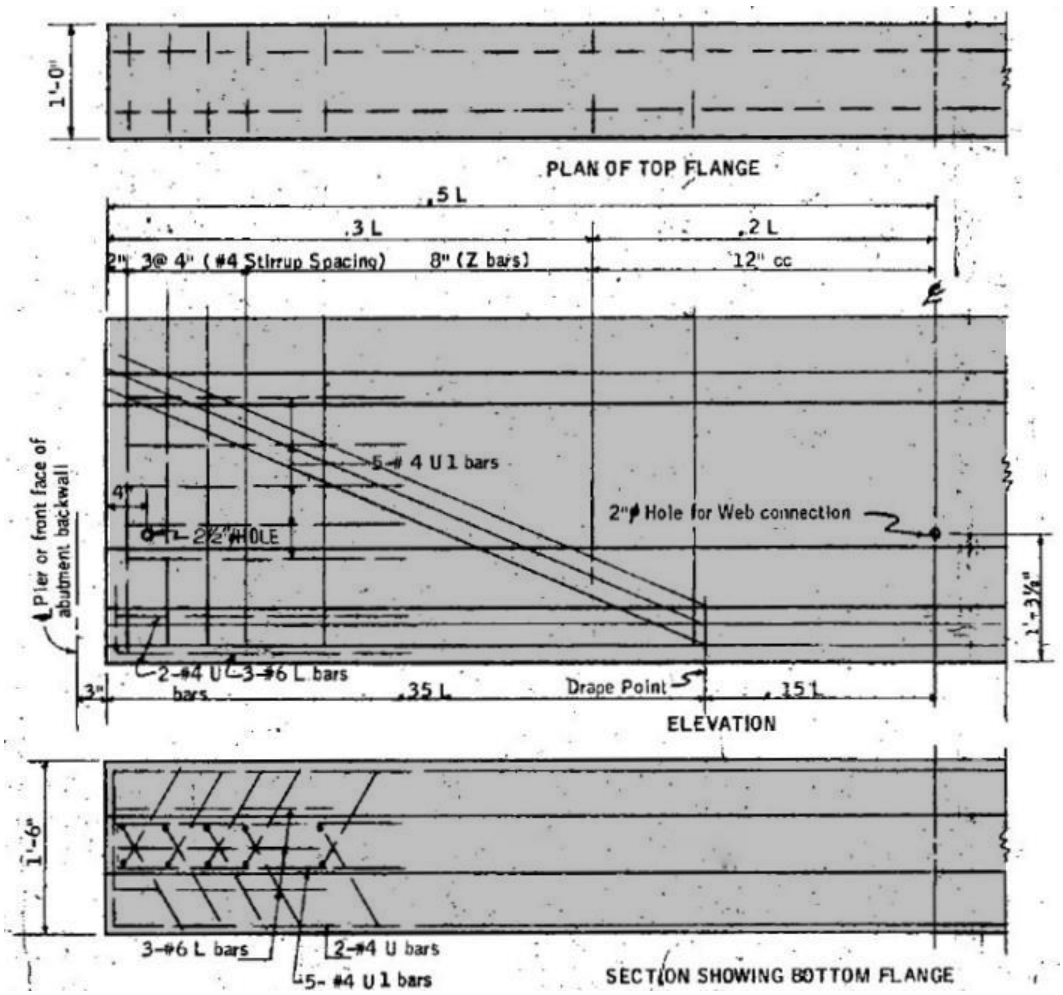

Figure 5.26 Original ODOT Reinforcing Diagram for Girder

Figure 5.27 North Boundary of North End Repair

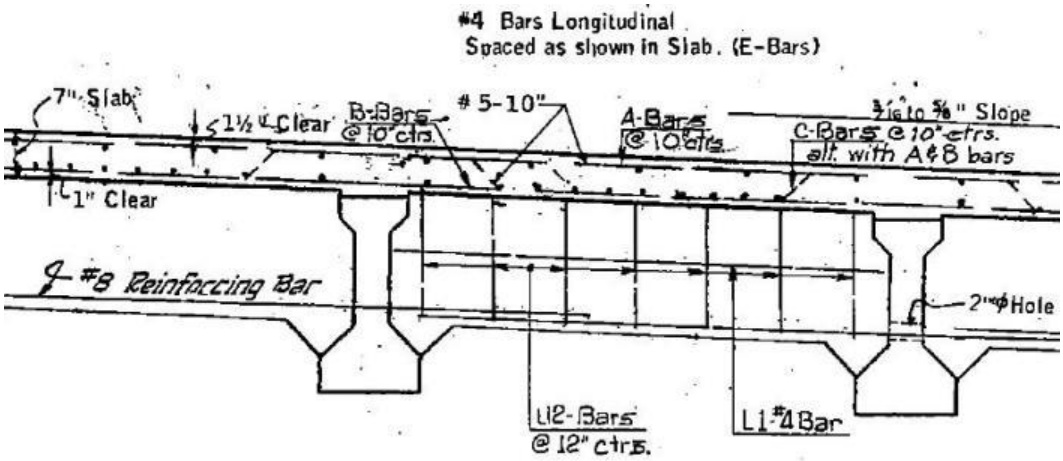

Figure 5.28 ODOT Typical Deck Reinforcing Diagram

Figure 5.29 Original Deck Reinforcement with Partial Concrete Demo

The first internal reinforcing repair was made to the straight strands at the bottom of the section. It was noted during the demolition of the north end, that all sixteen strands were in compression to some degree. The bottom strands were believed to be in compression due to either strand slip or from yielding in the original testing (Figure 5.30). To relieve the compression in the straight strands, GRABB-IT Cable Splices were installed. Before installing, thorough measurements of the hardware were taken and a model, shown in Figure 5.31, was constructed to configure a best-fit arrangement for the cable splices. Similarly to the south end repair, the cable splices needed to be offset in order to fit within the section. Once an arrangement was chosen, installation was conducted in accordance with the manufacturer's instructions. Initially, the manufacturer calls

for approximately 14 3/4 inch section of strand to be cut away and for the strand to be test-fitted into the “anchor body” of the assembly without the wedges in place so as to mark where the outer face of the “anchor body” lines up on the strand. That extent was marked on the strand and used as a datum to place the wedges. Once the wedges were placed, the spring was added and the threaded rod screwed into the “anchor body.” The threaded coupler and other threaded rod were added to the assembly and installed to the manufacture’s specified spacing and the “anchor body” for the other end was screwed into the threaded rod. This process was repeated for each of the ten straight strands. Once installed the assembly was tightened in the same sequence that the post-tensioning was applied in Section 5.3.6 until snug-tight.

Figure 5.30 Prestressing Tendons in Compression

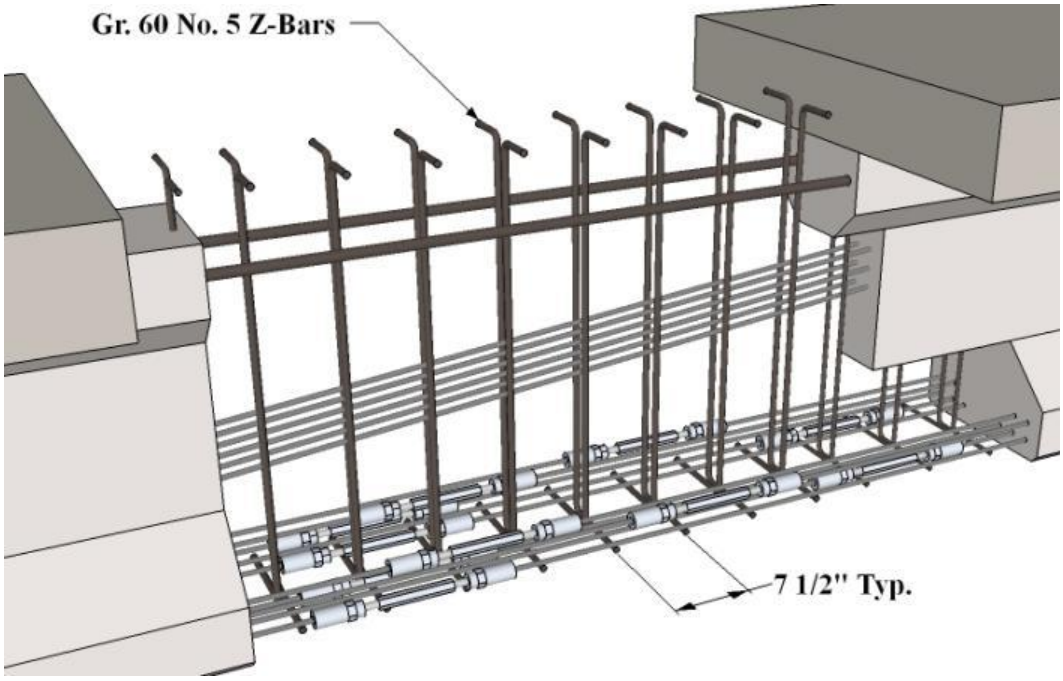

Figure 5.31 Internal Reinforcing SketchUp Model

After installing the cable splices, the replacement stirrups were constructed and mounted within the section. It was decided to not attempt to restore the prestressing to the harped strands and since the straight strands are only snug-tight, the repaired section would no longer be prestressed. Consequently, it was expected that there would be a drop in flexural and shear resistance that would have to be accounted for. With the previous failure mechanism being partially due to shear, an important aspect to the repair was to restore the shear resistance. Therefore, the loss in shear resistance from the loss in prestressing was calculated and would be accounted for in the replacement stirrup arrangement. The resulting setup was two Gr. 60, No. 5, Z-bars, identical to the

original stirrup shape, at 7 and 1/2 inches on center. The final arrangement of stirrups is shown in Figure 5.32.

Figure 5.32 North End Girder Internal Reinforcing

After the stirrups were placed, the final alteration to the internal reinforcing was to provide more concrete cover for the top longitudinal reinforcing bars in the girder. To achieve this, the bars were wrapped in single gauge wire, then a long steel rod was used to twist the wire, cinching the two bars towards each other. In doing so, the bars were bowed inward so that there would be at least one inch of cover over the buckled portion. Two No. 3 bars were bent into a C-shape around the top bars, securing them in place.

5.4.4 Placing the Girder Repair Concrete

In an effort to keep the original geometric properties of the girder, it was decided to cast the girder portion of the north end separate from the deck section. Originally, the deck was cast onto girders once they were in place and the top inch of the girder and the top of the Z-bars also extended into the deck. To mimic this process, the girder would be cast first, then the deck a few days later. The total volume of the girder repair is approximately 15.6 cubic feet of concrete, not accounting for the internal reinforcing. A total volume of 18 cubic feet was decided for casting day so that small scale cylinders could be cast in addition to the repair. Just as with the south end repair, all the materials were pre-batched and representative moisture samples were collected from the aggregates. All materials were sealed in their containers until mixing. The mixing procedure follows the steps previously outlined in Section 5.3.5 and conforming to ASTM C192. The formwork for the girder is open at the top, providing for easy access to pour the FR-SCC into the form. After the concrete was added to the repair section, six 6 inch by 12 inch cylinders were cast and a slump flow test was performed. The slump flow yielded 28.5 inches, which was the closest value to the target slump flow achieved in this study. At approximately one hour after casting, the top surface of the girder was roughened using masonry trowels to provide for improved bond between the girder and the deck (Figure 5.33).

Figure 5.33 Roughened Surface of North End Girder Portion

5.4.5 Repair of Deck Reinforcing

As the girder portion of the north repair was curing, the deck was prepared for casting. Using the formwork that was currently still attached to the girder as a brace, the deck form was attached and secured to the girder using threaded rods and two-inch-wide tow straps. The original transverse reinforcement was removed from the section and new No. 5 bars were their replacement. These new bars followed the same spacing as the original reinforcement; however, they featured 180° hooks at each end as opposed to being terminated at the face of the concrete as they were previously. On the east side, two longitudinal No. 4 bars were added in the corners of the transverse reinforcing bars. Figure 5.34 shows the final arrangement of internal reinforcing for the deck portion of the north repair.

Figure 5.34 Deck Reinforcing of North Repair

5.4.6 Placing the Deck Repair Concrete

The final stage for repairing the north end was to add the FR-SCC to the deck portion. The total repair volume for the deck portion was 15.1 cubic feet not accounting for the internal reinforcement. Since this amount is close to the volume for the girder portion, the mix for the girder portion was repeated. Material for 18 cubic feet of concrete was batched and mixed for the deck and another six 6 inch by 12 inch cylinders. Following the same mixing procedures as previously, the FR-SCC was placed into the deck forms and smoothed flat with trowels. After a few hours, the surface of the deck was resilient enough to place

wet burlap over the deck and a tarp over the burlap. This allowed the deck to moist cure for seven days, at which point the burlap was removed as well as the forms. Figure 5.35 shows the repair after removal of the formwork for the deck and girder.

Figure 5.35 West Side of Completed North End Repair

Chapter 6: Repaired Girder Testing & Results

With the girder repairs completed, the next step was to test the repaired sections and evaluate their performance. This chapter discusses the test preparations, arrangements, and performances of each test. The two tests performed follow the same conditions as the testing previously conducted by Murray as described in Chapter 4. A summary of the results of the load tests and the material strength tests are also presented at the end of the chapter.

6.1 South End Testing

6.1.1 Test Arrangement

In preparation for the girder's second set of testing, several aesthetic measures were put into place to both replicate original testing and to better identify the repair areas of the girder. First, the girder's west façade was repainted with a watered-down mixture of white latex paint. The coverage of the paint mixture was sufficient enough to coat the repaired areas, but thin enough to easily view the cracking from the original loading discussed in Chapter 4. White paint is a standard color and provides for better viewing conditions of propagating cracks during loading while also keeping to the aesthetics of Murray's testing. Next, the original, 6 inch gridlines were retraced and the centerline (midpoint of the girder span) was labeled along with each whole-foot gridline measured from the centerline. In Wirkman's research, discussed in Chapter 3, the repair beams had a red line marking the interface of the repair material and the control concrete.

Similarly, for this study, the interface between the repair material and the existing concrete was outlined with a red line on the west façade of the girder as shown in Figure 6.1. A full, photo elevation of the girder with the previously detailed enhancements is shown in Appendix B.

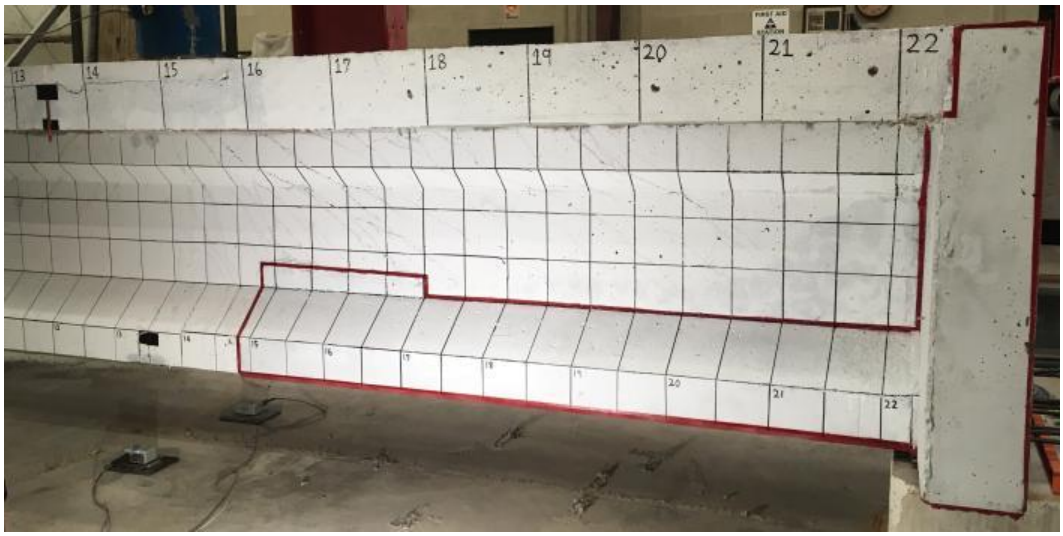

Figure 6.1 South End Repair Section Before Testing

The testing layout for the south end coincided with Murray's conditions for his "C1" test. The girder was supported at the southernmost end in such a way that the neoprene bearing pad aligned with the end diaphragm. The other support was positioned just past the midspan support, centered at 3.5 feet north of the centerline. And the load point was located 13.5 feet south of the centerline providing for a 9 foot length between the load point and southernmost support (Figure 6.2). This, again, matching the original test's *a/d* ratio of 3.0. Once the supports were in place, the girder was leveled by first placing a bubble level against the web in various locations along the girder to gauge how far

out-of-plumb the vertical axis of the girder was. Sieved sand was placed under the supports by placing a jack under the girder near the support and lifting the girder off the support temporarily until the sand could be added. A level was utilized to check orientation of the top surface of the concrete bearing block, then the girder was lowered back onto the bearing pad and the web was verified whether plumb or not a second time.

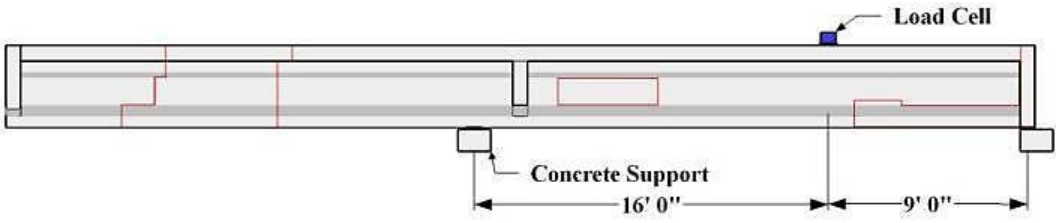

Figure 6.2 South End Test Support Conditions (West View)

Load was applied to the girder from a hydraulic ram mounted to a steel frame. This frame was fully adjustable in the vertical and horizontal axes by raising or lowering the cross members connecting the columns or by bolting the column bases to the strong floor which runs parallel to the length of the girder. Each test had the load frame positioned so that the ram was able to apply load without exceeding the stroke of the ram. The arrangement of the load transfer system is shown in Figure 6.3 and features a one-inch-thick steel plate that was leveled on a bed of sieved sand, then a load cell placed on top of the plate, and above the load cell was a load-leveler with a 4 inch, steel spacer.

Figure 6.3 Load Cell Arrangement

A few differences in the test set up, however, should be noted about the instrumentation used in the repair testing. In the original testing, linear variable differential transformers (LVDTs) were used to measure the end slip in the strands and the deflection of the bearing pads under load. Additionally, two wire potentiometers were attached to each side of the bottom bell directly in line with the plane of load, thus measuring the deflection during the test. This research

abandoned the use of LVDTs and only utilized the wire potentiometers in the same locations as was used in Murray's study. Not using the LVDTs should have minimal impact on the load-deflection plots during testing since the maximum recorded differential height of the bearing pads recorded in the original testing was approximately 1/16 inch. Attaching the wire potentiometers was achieved by shaping 12-gauge copper wire into a hook that was to hang from a 90 degree steel bracket. This steel bracket was epoxied to the face of the girder in such a way that the angle extending perpendicular to the girder surface was aligned with the bottom, horizontal gridline. Figure 6.4 displays the west façade of the girder with the aforementioned wire potentiometer set up. As a final measure, a scale was adhered to the west face of the deck accompanied by a laser-level mounted to the load frame to further gauge the vertical deflection throughout testing. An example of this is shown in Figure 6.5.

Figure 6.4 Wire Potentiometers for South End Test

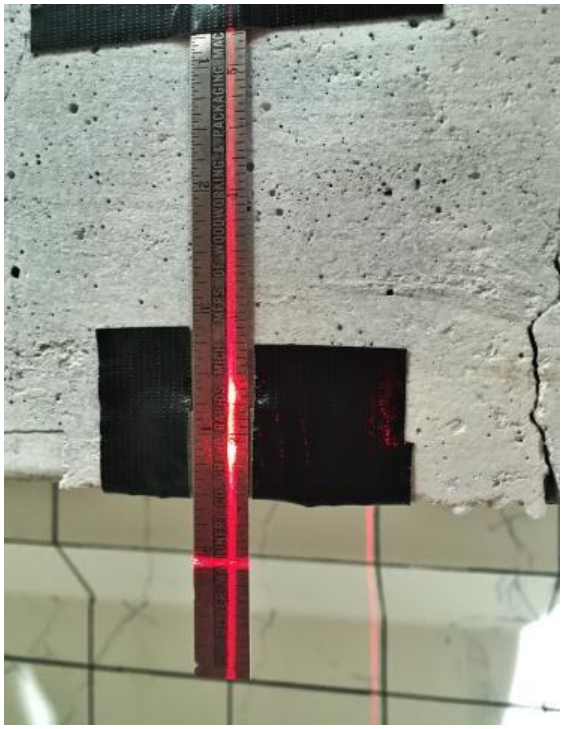

Figure 6.5 Laser Level Deflection Base Measurement

6.1.2 Testing Procedure

Load was incrementally applied in 10 kip increments in order to track the propagation of cracks throughout the section. Cracking was marked according to changes in the section that were visible to the naked eye. That is to say, if existing cracks appeared to be reopening, they were traced with a black marker for the length that they were reopening. Likewise, the same method would be followed for new cracks. Monitoring the reopening of existing cracks was best identified by observing when the newly-applied, thin layer of paint began to split. Being that there were many pre-existing cracks outside the repair zone, it is difficult to pinpoint when the section first began to crack or, rather, when cracks began to reopen. Yet, at 60 kips of applied load, existing cracks near the middle diaphragm began to spread into the web repair and a new crack began to form at the vertical interface of the south repair section and the existing concrete at an applied load of 80 kips. Existing cracks continued to reopen up to 130 kips, at which point the existing shear cracks in the web started to expand into the repair section at the south end of the girder. As the specimen continued to take load, more pre-existing shear cracks expanded into the repair area without trending along the interface of the repair. Some existing cracks lengthened to form fresh cracks in the existing concrete. The crack at the vertical interface located at the north end of the repair continually widened up to 3/4 inch at 249 kips, the maximum load, see Figure 6.6, at which point the girder ceased to take any additional load and the test was

stopped. Figure 6.7 illustrates the range of cracking for the testing of the south end repair.

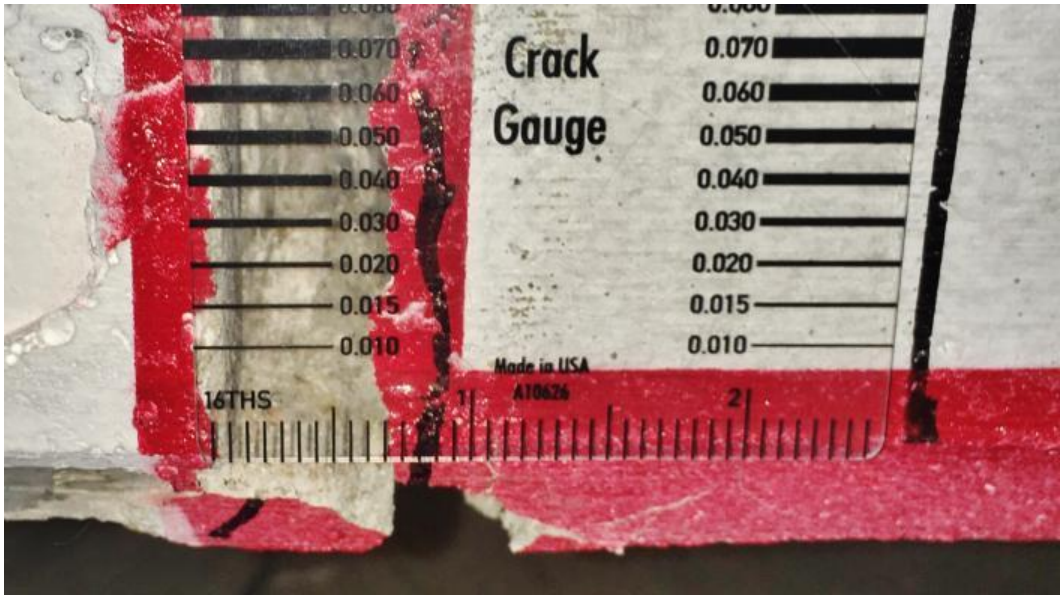

Figure 6.6 Crack Width of Repair Interface

Figure 6.7 Extent of Damage for South End Repair

6.1.3 Results

The maximum load, as mentioned previously, reached 249 kips at approximately 2 and 1/4 inches of average deflection, and load was continuously applied without actually increasing, until the maximum average deflection reached 2 and 5/8 inches under the same applied force. Testing was concluded at this deflection, as it seemed apparent that because the deck was not crushing, the strands were yielding. The vertical crack at the interface of the repair continued to grow, as discussed previously, confirming the elongation of the strands. The repair zone had several web-shear cracks that spread down, into the bottom bell, but did not fully extend to the bottom of the repair. Accordingly, it follows that the failure mechanism was purely flexural. Figure 6.8 shows the fully deflected state of the girder at the peak of testing.

Figure 6.8 South End Test at Maximum Deflection

6.2 North End Testing

6.2.1 Test Arrangement

Similarly with the relation between Murray's test "C1" and the south end testing, recreating the exact loading conditions as test "C2" was imperative to this study. The support conditions for the north end were selected based on a total span of 28 feet and an *a/d* ratio of 3.83. At the north end of the girder, a reinforced concrete block with dimensions of 18 inches x 24 inches x 12 inches (*l* x *w* x *h*) with a 8 inch x 18 inch x 1 inch neoprene bearing pad served as the support. This arrangement is typical of all supports for each test. Once the supports were in the correct location, they were leveled using sieved sand passing through a No. 16 sieve as previously described in Section 6.1.1. The support was centered on the north diaphragm and the load point was centered 11.5 feet south of the north support centerline. Figure 6.9 illustrates the support conditions for the north end test from a western vantage point. Similar to the south end test, the north end was only instrumented with two wire potentiometers and a load cell, no strain gauges or LVDT's were employed in the repair test. A photo of the test arrangement is shown in Figure 6.10.

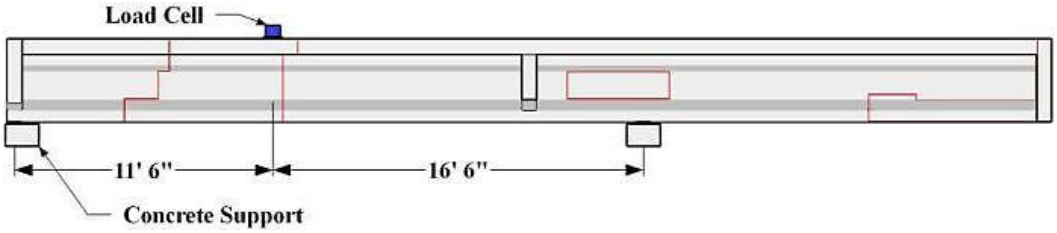

Figure 6.9 North End Test Support Conditions (West View)

Figure 6.10 North End Test Instrumentation

6.2.2 Testing Procedure

Following the same procedure as outlined in Section 6.1.2, 10 kip load increments were applied with crack propagation recorded between each step. Existing cracks were first recorded as reopening at 40 kips of applied load, which happens to be the load that the repair section exhibited its first cracks. These appeared to be flexural cracks due to their vertical trends through the bottom bell and web portion as shown in Figure 6.11. At an applied load of 80 kips, the flexural cracks in the repair zone began to orient themselves toward the load point, indicating flexure-shear behavior, however, most of the cracks in the repair appeared to traverse a limited lateral distance and tended to propagate more in a

vertical direction as opposed to the typical 45 degrees associated with shear behavior. As the load continued to increase, the quantity of flexure-shear cracks in the web of the repair grew. A large number of cracks formed in the bottom 6" of the girder following the 80 kip load increment and most spread in a direction parallel to the bottom strands (Figure 6.12). The interfaces of the repair with the existing concrete showed no signs of cracking and a few new and existing cracks crossed the interfacial plane without noticeable changes in orientation. Flexural cracks extended into the deck at 100 kips of applied load and continued to lengthen until the maximum recorded load but ceased to expand at the mid-height of the deck. The deck showed no signs of compressive failure despite having reopened a horizontal crack in the existing deck at the wearing layer interface on the east façade of the deck at an early load (Figure 6.13).

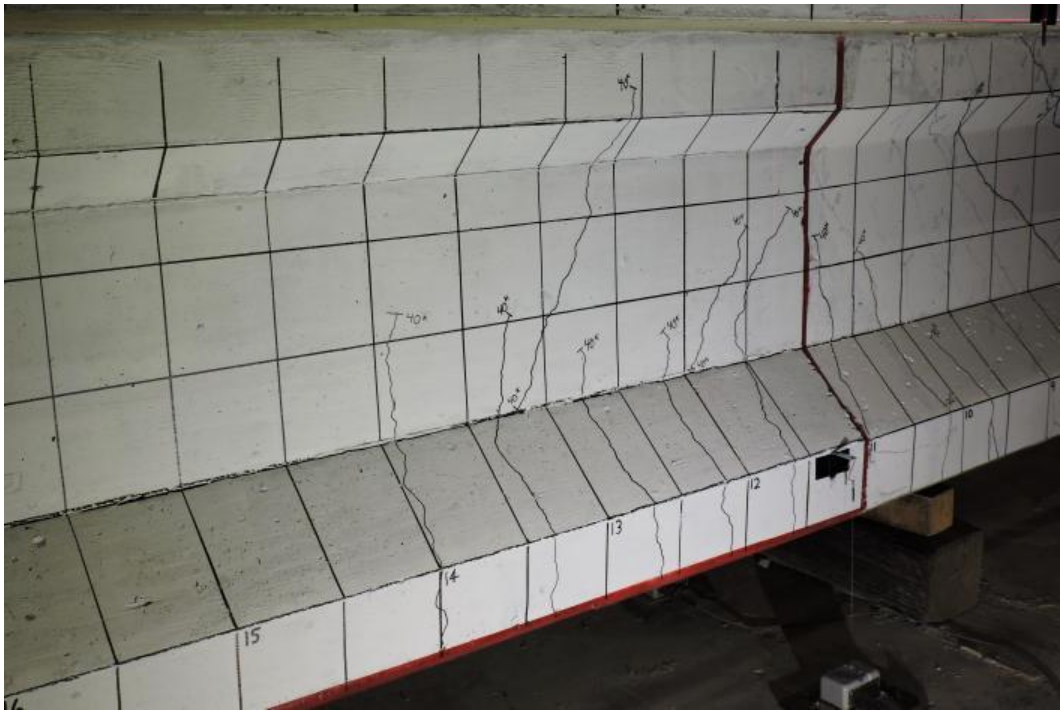

Figure 6.11 First Cracks in the Repair Zone

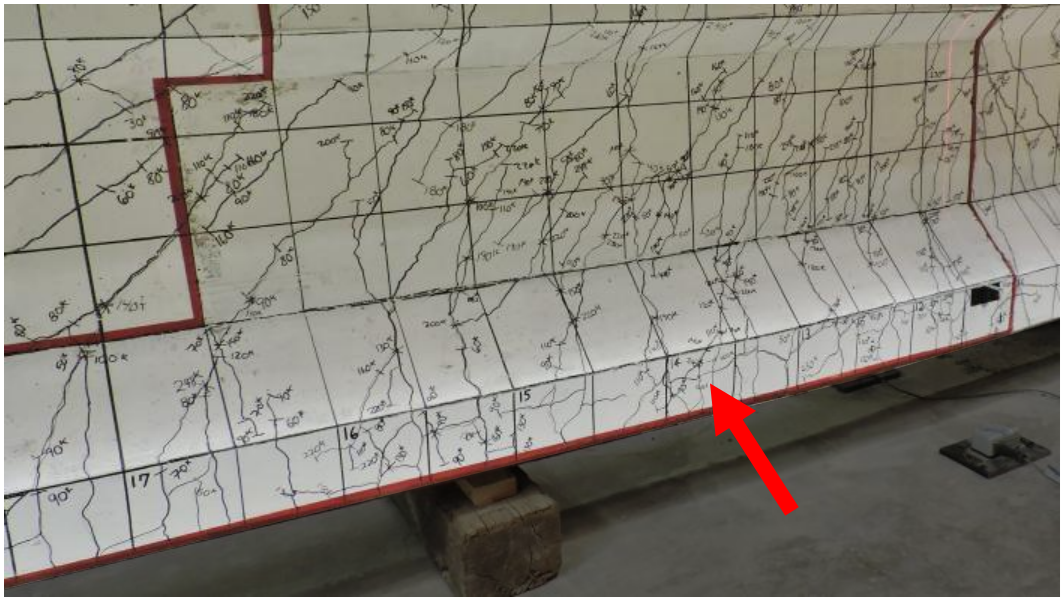

Figure 6.12 Shear-Bond Cracking in North Repair

Figure 6.13 Delamination of Wearing Layer During Repair Testing

6.2.3 Results

Under the maximum load able to be sustained by the girder, the deflection at the load point was 2 and 5/8 inches and continued to deflect under the same 249 kip load until the deflection reached approximately 3 and 1/8 inches of maximum deflection. After deflecting this additional 1/2 inch without an increase in resistance, the test was stopped and load was removed. Just as with the south end test, this end showed no signs of crushing in the deck and no signs of direct shear failure. Thus, it follows that the failure mechanism was flexural in nature. Within the repair zone most, if not all, of the cracks began as vertical, flexural cracks that, under increasing load, began to reorient themselves towards the load point as shown in Figure 6.14. Figure 6.15 shows the fully deflected girder during testing.

Figure 6.14 Post-Testing West Elevation of North End

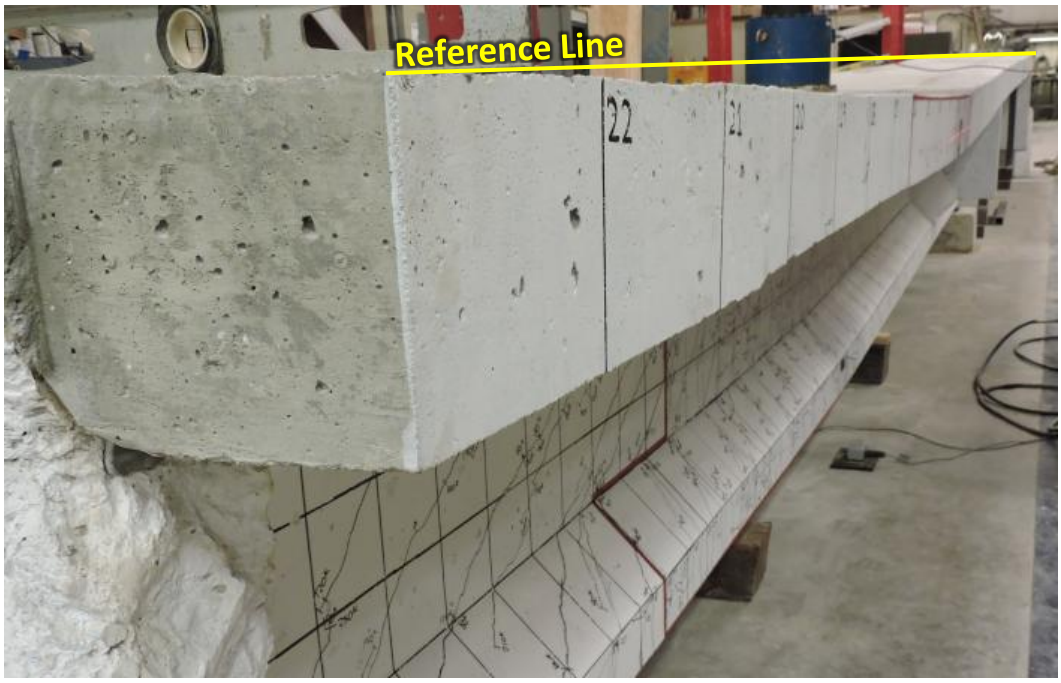

Figure 6.15 North End Test at Maximum Deflection

6.3 Summary of Results

6.3.1 Material Testing Results

For each repair section, compressive strength cylinders were cast so as to acquire the strength of the repair on the test date. The strengths for the south end repair yielded an average value of 7735 psi, though, it should be noted that when casting the south end only two cylinders were able to be cast at the ASTM acceptable size (6 inch by 12 inch) due to the lack of material. A third cylinder was cast, but it was the smaller 4 inch by 8 inch cylinder and the compressive strength from that cylinder was 864 psi below the next lowest strength obtained from the 6x12 cylinders. Consequently, the smaller cylinder and its strength data was excluded from the study.

The north end repair was a two-part construction in which the girder portion was cast first and the deck portion cast within a week after. The average compressive strength on the test day for the girder portion was 7614 psi and the deck returned an average of 6144 psi. The strength data for the material specimens is shown in Table 6.1.

Table 6.1 Repair Material Strength Data

Repair Section	28-Day Strength	Test Date Strength	Test Strength COV
South End Girder	-	7736 psi	3.10%
North End Girder	7662 psi	7614 psi	1.74%
North End Deck	6287 psi	6144 psi	2.16%

6.3.2 Load-Deflection Test Results

The load-deflection plots for both the south end and north end repair are shown in Figure 6.16 and Figure 6.17, respectively. The maximum loads for both tests was 249 kips with slightly different maximum deflections. A summary of the results are presented in Table 6.2 and post-repair testing elevations are provided in Appendix C.

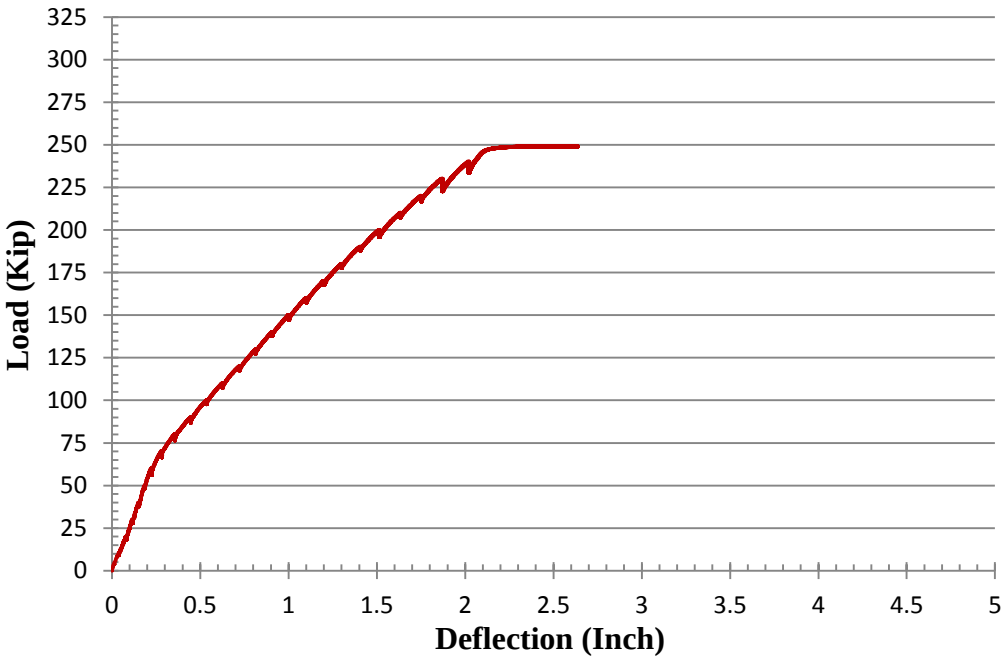

Figure 6.16 Load-Deflection Plot South End Repair Test

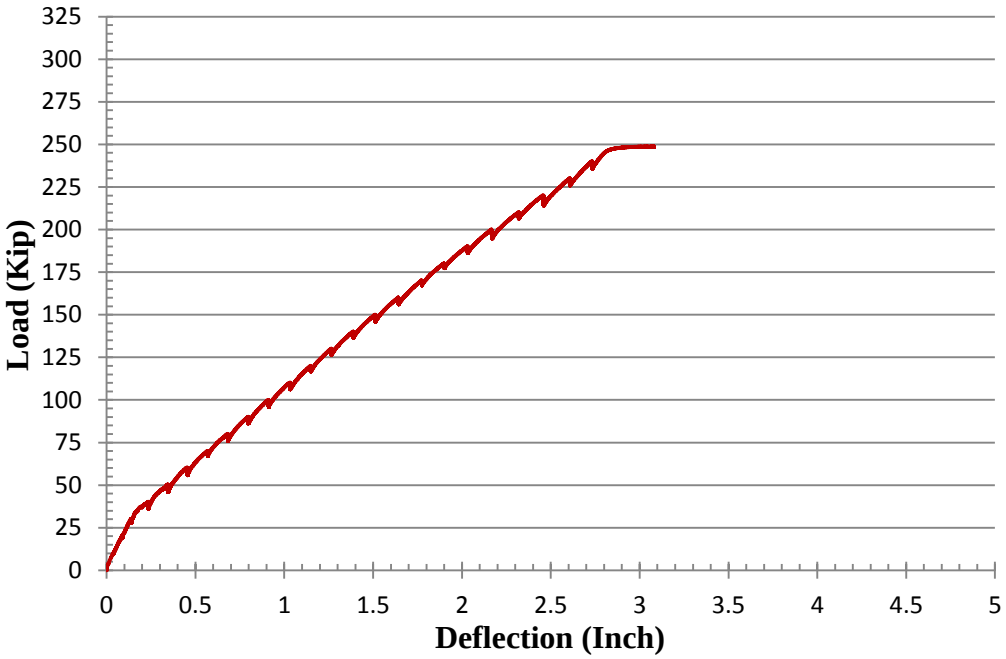

Figure 6.17 Load-Deflection Plot North End Repair Test

Table 6.2 Testing Results for Repaired Girder

Properties	South End	North End
Span	25 ft.	28 ft.
Cracking Load (Repair Zone)	80 kips	40 kips
Observed Cracking Moment	461 kip-ft.	271 kip-ft.
Max Load	249.0 kips	248.7 kips
Max Shear	159 kips	147 kips
Max Moment	1434 kip-ft.	1685 kip-ft.

Chapter 7: Comparative Analysis, Conclusions, & Recommendations

The primary goal for this study was to implement the previously developed fiber-reinforced, self-consolidating concrete (FR-SCC) presented in Chapter 3 as the repair material for a damaged AASHTO, Type II, bridge girder. This especially suited FR-SCC utilizes partial replacement of the cement with shrinkage compensating cementitious material without compromising strength or flow properties that are essential for repair and replacement of damaged concrete. After repairing the retired bridge girder, it was tested again and its performance comparatively analyzed based on its initial testing results. This chapter presents the comparative analysis between the original testing performed by Mr. Murray, as discussed in Chapter 4, and the repaired testing that is discussed in Chapter 6. Then, following the comparative analyses, conclusions of the study and recommendations for further studies relating to this research are given.

7.1 Comparative Analysis of Testing

7.1.1 South End & Test "C1"

The testing for the south end of the girder featured the same loading conditions as the original test, denoted by Murray as "Test C1," meaning that the load point and the support locations coincided with each other for both tests at the south end. A difference between the two tests were the instrumentation used. For the original testing, Murray utilized linear variable differential transformers

(LVDTs) to measure strand slip and the vertical deflection of the neoprene pads at the support. These parameters were not vital to this current study and, therefore, were not measured in the repair testing. Murray also employed wire potentiometers that were placed on each face of the girder at the load point to gauge the girder deflection as load was applied. This wire potentiometer arrangement was adopted for the repair testing, thus maintaining a consistent methodology in data collection.

Loading for both tests was applied in a series of 10 kip increments until failure. Negating the spalling at the south end support that occurred at 90 kips of applied load, the first cracks for the original testing of the south end appeared at 160 kips. The first sign of cracking for the repaired beam was difficult to pinpoint since there were pre-existing cracks outside of the repair zone, however, existing cracks first expanded into the repair zone at 60 kips, or approximately 38% of the cracking load in Murray's testing. First cracks for both tests appeared near the base of the top bell, just south of the middle diaphragm in the girder (Figure 7.1).

During the original testing, each load increment beyond the cracking load saw new or expanding web-shear cracks, whereas, for the repair test mostly existing web-shear cracks were observed to be reopening until the load reached 120 kips. At this load (approximately 48% of the maximum load for the repair testing), a majority of the flexural cracks began to reopen outside of the repair zone and the web-shear cracks directly above the south end repair zone started to extend down into the repair. It should be noted, though, that the crack at the

vertical interface of the repair and existing concrete continued to open at a consistent rate throughout loading. Flexural cracks were not observed in the original testing until the load reached 185 kips (approximately 58% of the maximum load) and the shear cracks were first observed to be entering the bottom bell region at this load. Then, upon reaching an applied load of 265 kips the shear cracks in the bottom bell propagated transversely, in the direction of the bottom straight strands in the area that was to be replaced by the repair. Murray states that this progression of cracking points to a bond failure for the bottom strands.

Conversely, the repair test displayed no signs suggesting bond failure and, furthermore, a majority of the shear cracks that did penetrate the repair zone did not reach the depth where the straight strands were located. The existing web-shear cracks in the repair girder did feature new extensions outside the repair zone as well but were not believed to be the source of failure. At failure, the original testing, as described by Murray, encompassed strand slip instigated by further propagation of shear cracking at the straight strand's depth. This, in turn, caused the deck to crush and delaminate resulting in increased deflection without an increase in load. The repaired girder, at failure, was observed to be an immediate increase in deflection at a consistent load with no crushing in the deck which is characteristic of an under-reinforced, flexural failure. The comparative results of the south end testing are listed in Table 7.1 and cracking plots for each test are located in the Appendix. The shear and moment values in Table 7.1 are calculated

from a simply supported arrangement of the girder in which the overhanging portion of the girder, beyond the northern support is ignored.

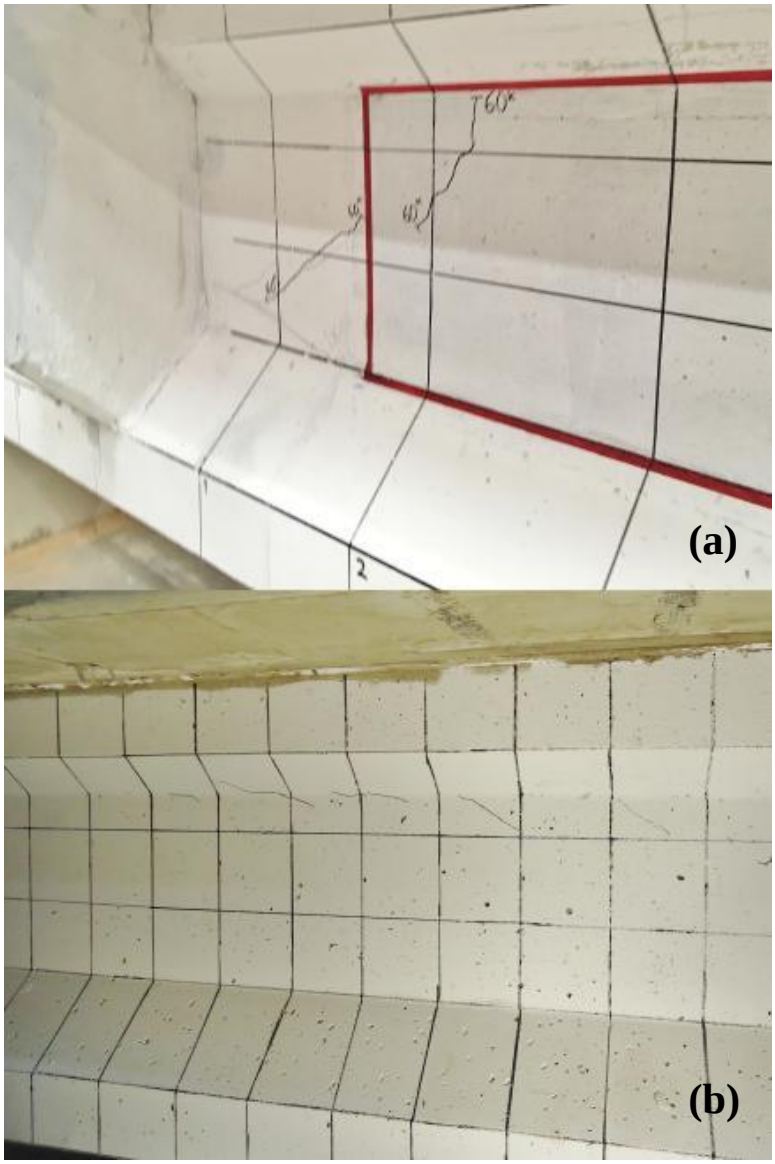

Figure 7.1 (a) First Cracks For South End Repair Beam Test (60 kips, West View); (b) First Cracks For Murray's "C1" Testing (160 kips, East View, Courtesy of Cameron Murray)

Table 7.1 South End Comparative Test Results

Properties	Test "C1"	South End Repair Test
Span	25 ft.	25 ft.
Cracking Load	160 kips	60 kips
Observed Cracking Moment	922 kip-ft	346 kip-ft
Max Load	318 kips	249 kips
Max Shear	204 kips	159 kips
Max Moment	1832 kip-ft	1434 kip-ft

With each iteration of testing, the toughness of the girder dropped and the slope of the load-deflection plot became more horizontal, which correlates to a decreasing stiffness, shown in Figure 7.2. That is to say, the stiffness for test "C1b" is higher than that of test "C1c" as well as the repair test. Thus, the toughness for test "C1b" is the highest, then "C1c," and the repair test with the lowest toughness as well as the lowest stiffness.

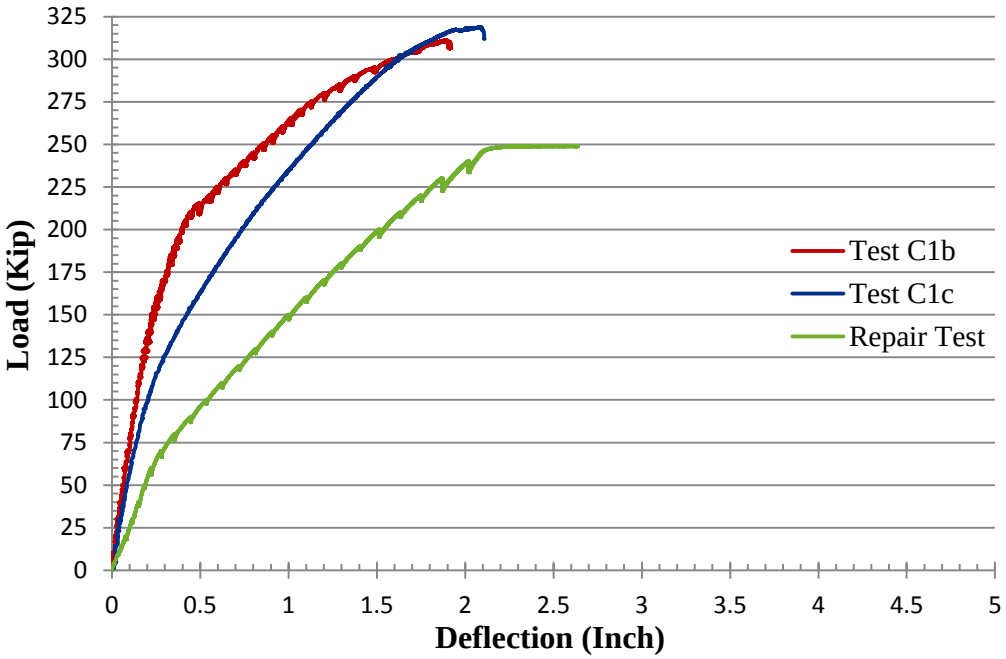

Figure 7.2 Load vs. Deflection Plot of Original and Repair Testing of South End of Girder

7.1.2 North End & Test "C2"

The support and loading conditions for the north end repair test were identical to Murray's original "C2" test conditions; and just as with the testing for the south end, the north end repair test featured only the two wire potentiometers at the location the load was applied and none of the LVDTs that the original testing included. Again, the strand slip and deflection of the neoprene pads were not relevant to this research and, therefore, excluded from the repair testing.

Both the repair test and Murray's tests were loaded 10 kips at a time in order to monitor crack propagation. The first recorded cracks for the original testing appeared at an applied load of 150 kips (about 50% of the maximum load). For the repair test, the first cracks in the repair zone were recorded at 40 kips

(approximately 16% of the maximum load of the repair test), equating to about 27% of the cracking load for the original testing. These cracks were flexural, located in the bottom bell of the repair section and the first cracks for Murray's tests appeared as web-shear cracks near the northern support as shown in Figure 7.3.

Then, at the next load increment, 160 kips (53% of the maximum load), flexural cracks first appeared and continued to multiply and grow until their extension reached the deck at 190 kips (63% of the maximum load). A majority of the initial cracking of the north end repair test were flexural, though, there were a few web-shear cracks that formed after 60 kips (about 24% of the maximum repair load). Also, just as with the south end repair test, the north end repair test had existing cracks that reopened outside of the repair zone throughout the test. At 80 kips (32% of the maximum load) the flexural cracks reached the deck in the repair zone and web-shear cracks outside the repair began to penetrate the repair. At approximately 110 kips, horizontal cracks began to form at the depth of the straight strands and continued to develop during the remainder of testing along with flexure and web-shear cracks in the repair section. Then, when approaching failure for the repaired girder, there was the presence of numerous flexural, web-shear, and horizontal debonding cracks and increased deflection as the load reached its maximum value. The plot for the repair test shows an identical plot trend to the repair test for the south end suggesting that the failure mechanism is also flexural. The original testing failure mechanism was recorded as being either

a compression-shear failure or a flexural failure. Although, when performing the demolition of the north end, it was uncovered that there was a clearly defined plane of shear that extended through the deck to the load point. This shear plane was defined by the presence of large cracks and buckling of the longitudinal bars exactly in line with the shear plane shown in Figure 7.4.

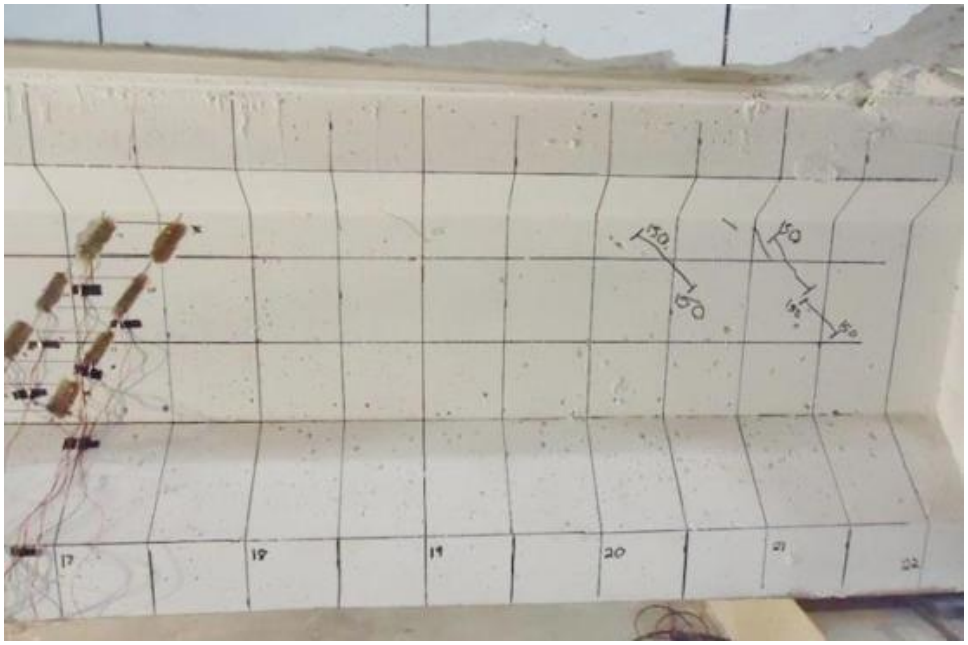

Figure 7.3 First Cracks for Murray's North End Testing (150 kips, East View, Courtesy of Cameron Murray)

Figure 7.4 North End Shear Plane (Yellow Line) Discovered Mid-Demolition

Analogous to the south end testing, Figure 7.5 illustrates that with each progression of testing, the stiffness and toughness of the girder decreases. Test "C2a" exhibited the highest stiffness and, thus, the dominating value of toughness; the repair test matched the stiffness of test "C2b" until the cracking load, at which point the stiffness changed to a linear plot much like the repair testing for the south end repair. It should be noted that both repair tests, north and south, attained their maximum load at approximately the same deflection as each end's original testing that was conducted by Murray. The comparative testing results for the north end are given in Table 7.2 and a plot of the extent of cracking for the original and repair testing are presented in the Appendix. The values in Table 7.2 are derived from a simply supported arrangement, neglecting the influence of the overhanging portion of the girder.

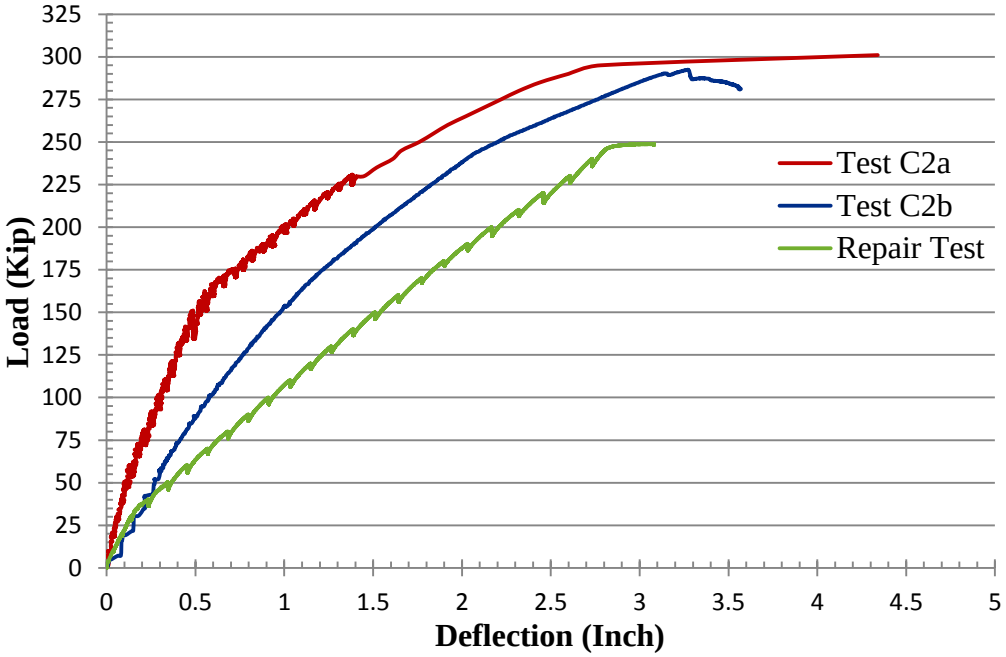

Figure 7.5 Load vs. Deflection Plot of Original and Repair Testing of North End of Girder

Table 7.2 North End Comparative Test Results

Properties	Test C2	South End Repair Test
Span	28 ft.	28 ft.
Cracking Load	150 kips	40 kips
Observed Cracking Moment	771 kip-ft	271 kip-ft
Max Load	301 kips	249 kips
Max Shear	177 kips	147 kips
Max Moment	2040 kip-ft	1685 kip-ft

7.2 Conclusions

7.2.1 Material Properties

The reported average strengths from Murray's analysis were 7,180 psi for the girder and 6,060 psi for the deck. Likewise, for the repair, the average strengths were reported on testing day as 7,736 psi for the south end repair, 7,614 psi for the north end girder portion, and 6,144 psi for the deck. The strength differences of the repair materials are all within 7.7% of the specimen's originally tested average strengths, which is within the acceptable range for "single-operator precision" as defined by ASTM C39/C39M – 17a, the "*Standard Test Method for Compressive Strength of Cylindrical Concrete Specimens*." Hence, it follows that the FR-SCC repair material was of an acceptable and comparable compressive strength to that of the originally cast concrete for the girder and deck. Table 7.3 shows the relationship for strengths between the existing concrete strength and the repair material strengths. Additional information on the material strengths for the girder and the internal reinforcement are covered in Chapter 4 for Murray's testing and Chapter 6 for the repair material strengths.

Table 7.3 Comparative Girder Concrete Compressive Strengths

Property \ Location	Average Test Day Strength	Difference From Existing Concrete Strength
Existing Concrete, Girder	7180 psi	--
Existing Concrete, Deck	6060 psi	--
South End Repair Concrete	7736 psi	7.74%
North End Repair Concrete, Girder	7614 psi	6.04%
North End Repair Concrete, Deck	6144 psi	1.39%

An imperative aspect of this study that also was a focal point for the research and development that was a precursor to this study was the applicability of the FR-SCC as a viable repair material in the field. In Wirkman's study, he found that the mix used in this study was able to flow under its own weight much like conventional self-consolidating concrete mixtures and that its passing and fill abilities were well equipped for repair applications. When considering the flow passage and obstacles of the repair zones in this study (see Chapter 5 for additional details pertaining to the repair process), the aforementioned mix characteristics were reverberated for this research.

7.2.2 Performance of the Repaired Girder

In addition to the individual properties of the FR-SCC, another essential aspect to the study and evaluation of the repair material was its influence on the performance of testing conducted on a previously tested AASHTO, Type II,

bridge girder with a composite deck. During the south end repair test, a crack at the vertical interface between the repair concrete and the existing concrete formed at the cracking load, which was just south of the applied load. According to Figure 7.2, this is the point in the loading that the load-deflection plot changes slope, and proceeds to increase linearly as load is applied. When taking into account that this linear stiffness continues until failure and that the crack that appeared at the vertical interface of the repair and existing concrete widened throughout testing, it is clear that the strength of the strands were key to the overall capacity, i.e., the strands were responsible for taking the full tension force of the internal moment; that with the increase in load, the strands were elongating, elastically, until they reached their elastic limit and began undergoing plastic elongation. This can be supported by calculating the stress in the strands from the maximum load attained from the test and using the strain compatibility method equations along with stress/strain relationships.

The maximum load for the south end repair test was 78% of the maximum load recorded for the original testing and each of the failure mechanisms were different. Murray's testing of the south end resulted in a bond-shear failure that resulted in a large volume of concrete dislodging from the girder, whereas, the failure mechanism for the repair test was flexural and the failure occurred at the boundary of the repair, not in the repair zone. The repair testing of the south end left the girder in a fractured, but intact state that, when unloaded, the permanent deflection of the girder was 1/2 inch below the pretested, non-deflected state. And

so it draws that the repair was able to mitigate the shear stresses while providing for a ductile failure. Granted that, in Murray's discussion of the south end testing, he states that once the bond of the straight strands was lost, the shear capacity of the girder was solely dependent on the resistance of the shear stirrups or the capacity dwindles. Because the repair included post-tensioning that was anchored at the southernmost end of the girder, the repaired girder was likely to have never experienced the same bond-induced, shear failure that the original testing exhibited. As the girder was loaded for each repair test, it appeared that the internal stresses of loading were redirected to the repair zone and other sections of the girder that were less cracked. This was due to the flexible nature of a cracked section adjacent to a stiff, uncracked section. It is possible that if the repair zone had terminated farther from the load point, that the girder could have achieved a higher stiffness for the same loading. Still, the maximum load would be identical once the cracks fully penetrated the repair section since the unrepaired portion of the girder was already cracked.

Similarly to the load-deflection plot for the south end repair, the north end repair test features a clear change in slope at the cracking load, shown in Figure 7.5. The plot also shows that before this stiffness change, the slope of the plot for the repair test closely aligns with the slope of the "C2b" test plot. After the stiffness change, the plot increases linearly until failure much like the repair test for the south end. This leads to suggest that when the cracks propagated, the strands debonded from the concrete creating a similar resisting internal moment to

the south end. This internal moment is characterized by an under-reinforced section where the ten straight strands at the bottom are taking the full tensile stress. It can be concluded that this points to a flexural failure, but it is believed that the horizontal cracks at the depth of the straight strands were causation for debonding of the strands that, in turn, resulted in a flexural failure. When comparing the slope of both repair tests beyond the cracking load, the stiffness for the north end is less than that of the south end. This can be accounted for when considering the effects of a larger span for the north end than the south end.

All things considered, each repair test successfully restored the capacity of the girder to approximately 80% of its previously tested capacities. This equates to a shear value that is on average 65 kips higher than the original demand for both the North and South end tests. Thus, the repair was able to restore the girder to 175% the original demand (Floyd et al, 2016). Moreover, the repair was able to mitigate the original shear-based, failures that resulted from the first testing even though the load conditions were designed to incite shear failure. The crack propagation of the repair material was evenly dispersed and there were no signs of delamination at the boundaries of the repair (excluding the vertical interface of the south end repair). Therefore, the FR-SCC is a viable solution for a repair material that exhibits comparable mechanical properties to existing self-consolidating concrete mixes used for existing structures.

7.3 Recommendations

Currently there are a finite number of published studies detailing the potential for structural repair of concrete using FR-SCC, despite the necessity for solutions to the subpar status of current infrastructure. In addition to this study, it comes as a recommendation that further attention to be brought to the method of application for FR-SCC as a repair material as well as the mixture of the FR-SCC, itself.

7.3.1 Application Recommendations

First and foremost, it is suggested that more full-scale testing be performed on damaged, structural members. A wider variety of damage such as lateral impact damage and corrosion should be investigated as potential specimens for repair. In addition to these other methods of damage, the location of the applied damage and the effects of where along the span of the member should be analyzed. Axially loaded members could be subjected to damage and should be investigated for the use of FR-SCC as a repair material.

This study limited the repair area to only replace a designated extent of damage received during the original testing without regard to the loading location. As mentioned in the previous sections, the farther the boundary of the repair was from the load, there could be a potential of a stiffer performance of the section. As such, it is suggested that variable lengths of repairs be evaluated to determine

what axial length from the load should the repair extend, if any, to provide the best performance.

7.3.2 Continued FR-SCC Development Recommendations

With the FR-SCC design that was used for this study, there was a very small 10 minute window of use before additional set-retarder must be added. However, this window was only possible for ideal weather conditions. If the ambient weather was particularly dry, hot, or a combination of the two, then the set-up time for the mix was shorter, limiting the workability time. If the mix was not in place before reaching the end of its window of workability, then it displayed an exponential decrease in its characteristic self-consolidating properties. The method used for this study to extend the workability time was to re-dose the retarder (citric acid) to the volume of concrete still in the mixer. Thus, to provide for a wider window of workability, the investigation of other set-retarding admixtures should be evaluated with a secondary goal of producing a less environmentally-sensitive mix design.

In the research and development of the FR-SCC design, Wirkman suggested further exploration of various other fibers and their effects on the mix. Due to changing markets and continual refinement and development of concrete, there are numerous fibers available. There is probability that the fibers currently used will be replaced or withdrawn from manufacturing. For the sake of mix versatility and to minimize performance variability between different fibers,

research exploring the effects of other substitutions of reinforcing fibers comes as a recommendation.

Bibliography

Alkhrdaji, Tarek, Ph.D., P.E. "Strengthening of Concrete Structures Using FRP Composites." Building Blocks. STRUCTURE Magazine, June 2015. Web. 6 Apr. 2016. www.structuremag.org/?p=8643.

ASCE. "2017 ASCE Infrastructure Report Card." Bridge Infrastructure | Structurally Deficient Bridges | ASCE's 2017 Infrastructure Report Card, www.infrastructurereportcard.org/cat-item/bridges/.

Federal Highway Administration. "Bridges & Structures." Bridge Condition by Functional Classification Count 2017, U.S. Department of Transportation/Federal Highway Administration, 31 Dec. 2017, 2/28/2018, www.fhwa.dot.gov/bridge/nbi/no10/fccount17.cfm.

Floyd, Royce W., et al. *Understanding the Behavior of Prestressed Girders after Years of Service*. Office of Research and Implementation, Oklahoma DOT, 2016, pp. 50–61, *Understanding the Behavior of Prestressed Girders after Years of Service*.

Guettala, & Abibsi. (2006). *Corrosion degradation and repair of a concrete bridge*. Materials and Structures, 39(4), 471-478.

INDOT. *Rebuilding of Rockville Road over 465*, Indiana Department of Transportation, 1 May 2017, www.in.gov/indot/3613.htm.

Kassimi, Fodhil. *Development and Performance of Fiber-Reinforced Self-Consolidating Concrete for Repair Applications*, Universite de Sherbrooke (Canada), Ann Arbor, 2013. *ProQuest*, https://search.proquest.com/docview/1520158859?accountid=12964.

Murray, Cameron, et al. "Understanding Ultimate Shear Behavior of Prestressed Concrete Girder Bridges as a System Through Experimental Testing and Analytical Methods." *Understanding Ultimate Shear Behavior of Prestressed Concrete Girder Bridges as a System Through Experimental Testing and Analytical Methods*, 2017.

Nossoni, Goli, and Ronald S. Harichandran. "Improved Repair of Concrete Structures Using Polymer Concrete Patch and FRP Overlay." *Journal of Materials in Civil Engineering*, vol. 22, no. 4, Apr. 2010, doi:10.1061/(ASCE)MT.1943-5533.0000020.

Shield, Carol, and Paul Bergson. *BR27568 – Experimental Shear Capacity Comparison Between Repaired and Unrepaired Girder Ends*. Minnesota

Department of Transportation, 2018, *BR27568 – Experimental Shear Capacity Comparison Between Repaired and Unrepaired Girder Ends*.

U.S. Dept. of Transportation. "Policy and Government Affairs." *2013 Conditions and Performance*. Federal Highway Administration, 7 Nov. 2014. Web. 07 Mar. 2016.

Wirkman, Corey Michael. "Performance of Fiber-Reinforced Self-Consolidating Concrete for Repair of Bridge Sub-Structures." *Performance of Fiber-Reinforced Self-Consolidating Concrete for Repair of Bridge Sub-Structures*, 2016.

Woodson, R. Dodge. (2009). *Concrete Structures - Protection, Repair and Rehabilitation*. Elsevier. https://app.knovel.com/hotlink/toc/id:kpCSPRR001/concrete-structures-protection/concrete-structures-protection.

Wu-Jian Long, Kamal Henri Khayat, Guillaume Lemieux, Soo-Duck Hwang, & Feng Xing. (2014). *Pull-Out Strength and Bond Behavior of Prestressing Strands in Prestressed Self-Consolidating Concrete*. Materials, 7(10), 6930-6946.

Zobel, Robert Steven. "Evaluation and Repair of Impact Damaged Pre-Stressed Concrete Bridge Girders." Order No. 9633342 The University of Texas at Austin, 1996. Ann Arbor: *ProQuest.* Web. 25 Jan. 2016.

Appendix A – Girder Survey Data

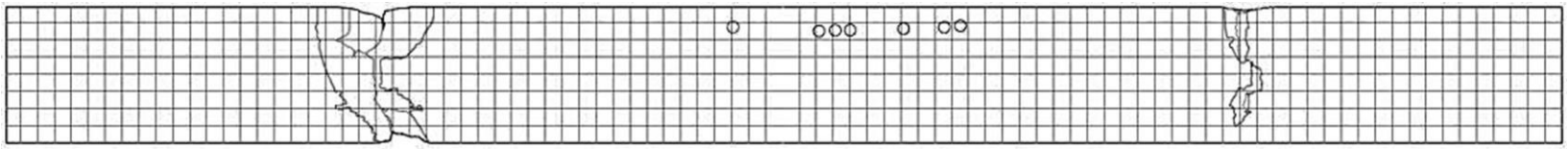

Figure A.1 Deck Survey Plot From Initial Testing

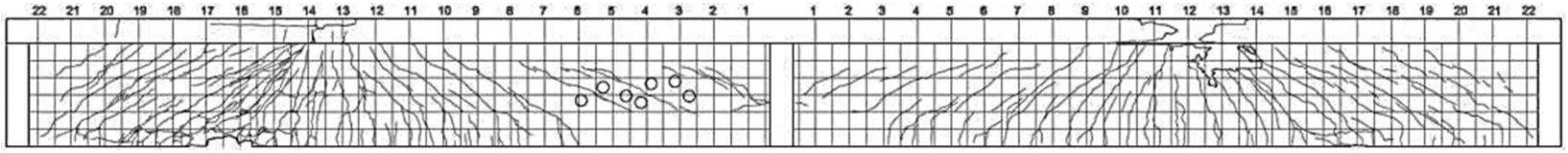

Figure A.2 East Elevation Survey From Initial Testing

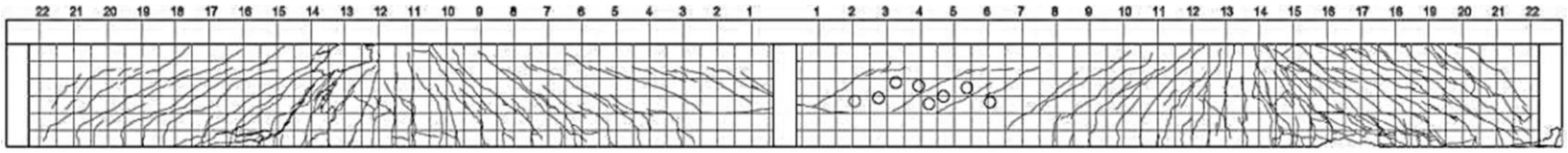

Figure A.3 West Elevation Survey From Initial Testing

Figure A.4 West Photographic Elevation From Initial Testing

Figure A.5 West Photographic Elevation From Repair Testing

Figure A.6 Enlarged West Photographic Elevation From Initial Testing (North End)

Figure A.7 Enlarged West Photographic Elevation From Initial Testing (South End)

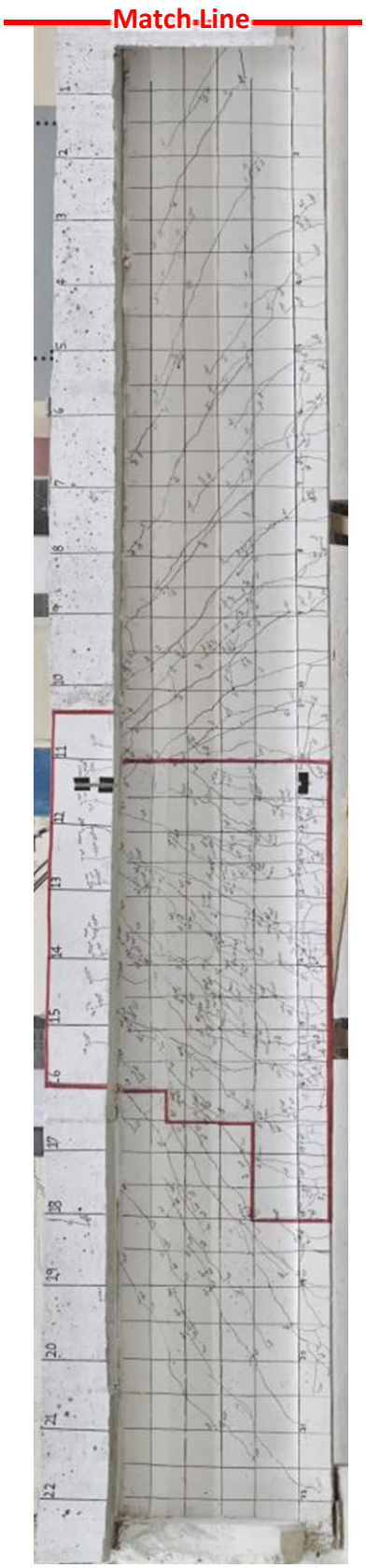

Figure A.8 Enlarged West Photographic Elevation From Repair Testing (North End)

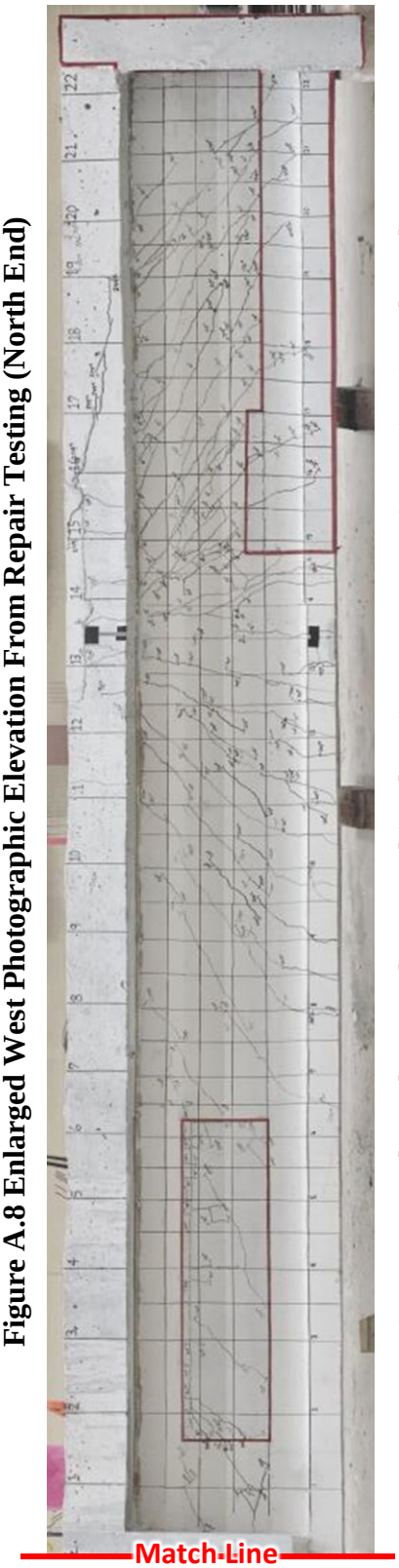

Figure A.9 Enlarged West Photographic Elevation From Repair Testing (South End)

Appendix B – Photos of Concrete Removal

Figure B.1 Loose Concrete Removed From South End With Hammer

Figure B.2 One-Inch Boundary Line Cut With Hand Grinder (South End)

Figure B.3 North End Bottom Bell & Loose Concrete Removal

Figure B.4 Removal of Deck Concrete Using an Impact Hammer

Appendix C – Photos of Internal Reinforcing Repair

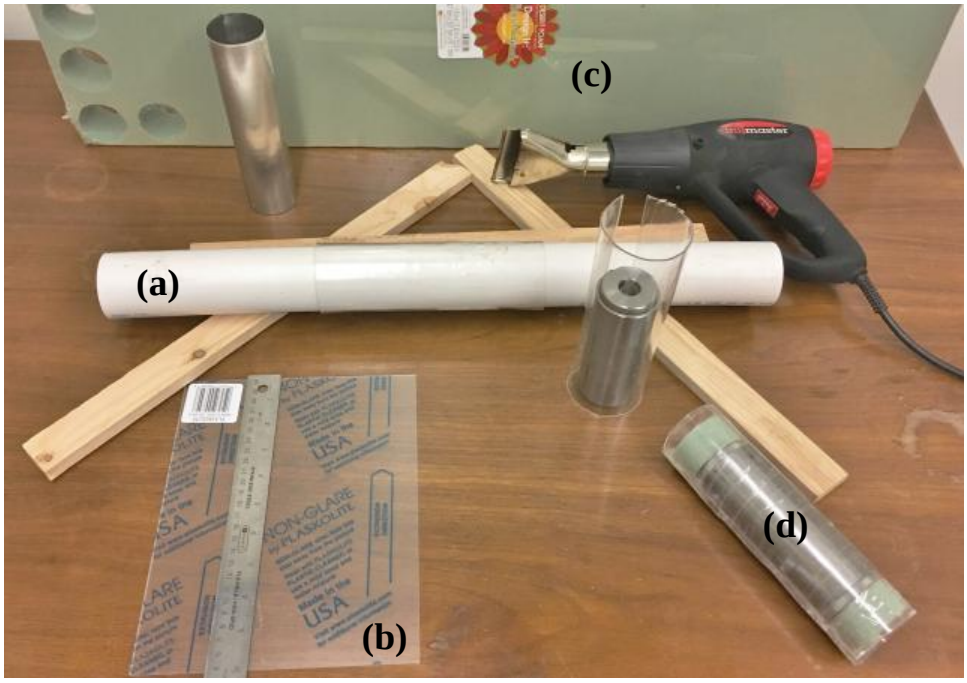

Figure C.1 Coupler Housing Construction; (a) PVC Mold ; (b) Acrylic Sheet Before Molding; (c) Crushable Foam Cutouts; (d) Final Product

Figure C.2 Post-Tensioning Anchorage Installed to Formwork With Insulating Foam to Seal the Backside

Figure C.3 Bent Longitudinal Reinforcing of North End Repair

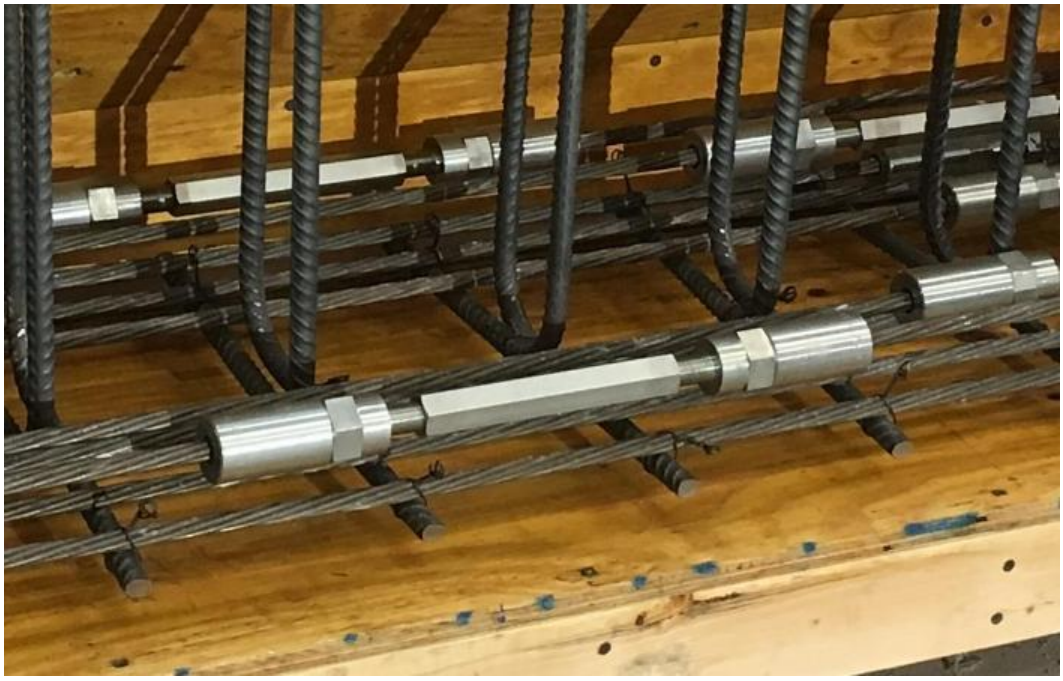

Figure C.4 Turnbuckle Splices for North End Straight Strands

Appendix D – Supplemental Repair Photos

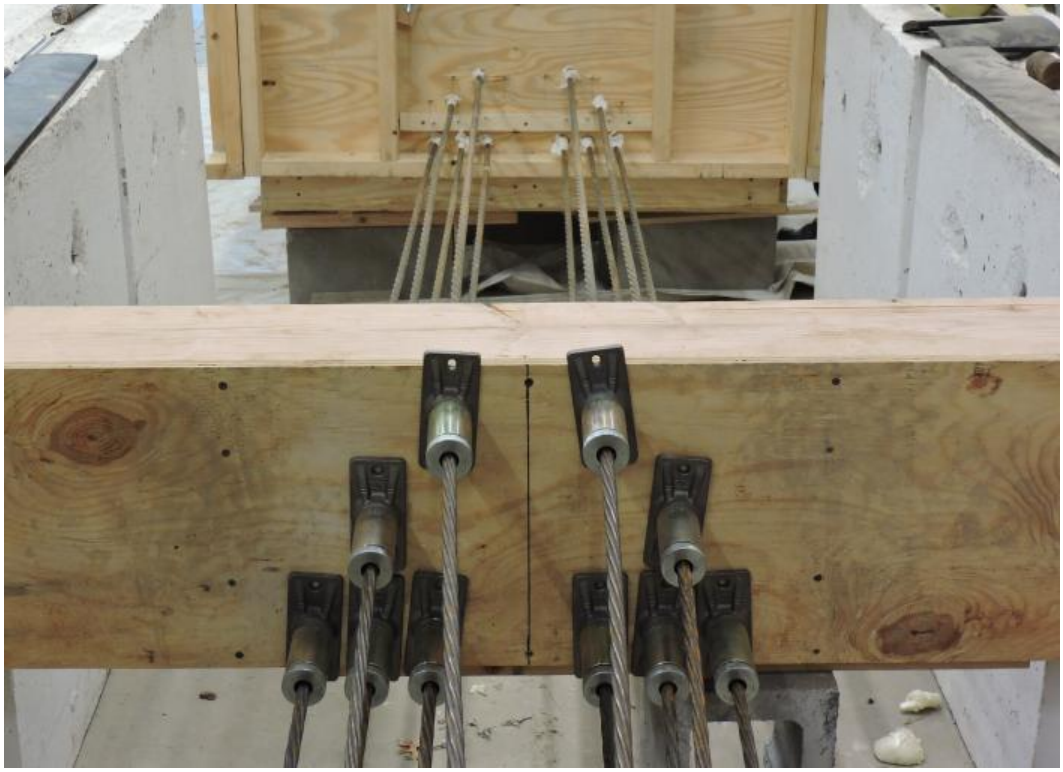

Figure D.1 Post-Tensioning Anchor Head

Figure D.2 Adding Cementitious Material During the Mixing Process

Figure D.3 Adding the FR-SCC Repair Material to the South End

Figure D.4 Slump Flow Test Results of FR-SCC